Geosci. Model Dev. Discuss., https://doi.org/10.5194/gmd-2018-322
Manuscript under review for journal Geosci. Model Dev.
Discussion started: 25 March 2019

Geoscientific Model Development Discussions

Title :
ORCHIDEE MICT-LEAK (r5459), a global model for the production, transport and transformation of dissolved organic carbon from Arctic permafrost regions, Part 2: Model evaluation over the Lena River basin.

Authors:
Simon P.K. Bowring[1], Ronny Lauerwald[2], Bertrand Guenet[1], Dan Zhu[1], Matthieu Guimberteau[1,3], Pierre Regnier[2], Ardalan Tootchi[3], Agnès Ducharne[3], Philippe Ciais[1]

Affiliations:
[1] Laboratoire des Sciences du Climat et de l'Environnement, LSCE, CEA, CNRS, UVSQ, 91191 Gif Sur Yvette, France
[2] Department of Geoscience, Environment & Society, Université Libre de Bruxelles, Bruxelles, Belgium
[3] Sorbonne Université, CNRS, EPHE, Milieux environnementaux, transferts et interaction dans les hydrosystèmes et les sols, Metis, 75005 Paris, France

Abstract
In this second part of a two-part study, we perform a simulation of the carbon and water budget of the Lena catchment with the land surface model ORCHIDEE MICT-LEAK, enabled to simulate dissolved organic carbon (DOC) production in soils and its transport and fate in high latitudes inland waters. The model results are evaluated in their ability to reproduce the fluxes of DOC and carbon dioxide (CO_2) along the soil-inland water continuum, and the exchange of CO_2 with the atmosphere, including the evasion outgassing of CO_2 from inland waters. We present simulation results over years 1901-2007, and show that the model is able to broadly reproduce observed state variables and their emergent properties across a range of interacting physical and biogeochemical processes, including: 1) Net primary production (NPP), respiration and riverine hydrologic amplitude, seasonality and inter-annual variation; 2) DOC concentrations, bulk annual flow and their volumetric attribution at the sub-catchment level; 3) High headwater versus downstream CO_2 evasion, an emergent phenomenon consistent with observations over a spectrum of high latitude observational studies. (4) These quantities obey emergent relationships with environmental variables like air temperature and topographic slope that have been described in the literature. This gives us confidence in reporting the following additional findings: (5) Of the ~34TgC yr^{-1} left over as input to terrestrial and aquatic systems after NPP is diminished by heterotrophic respiration, 7 TgC yr^{-1} is leached and transported into the aquatic system. Of this, over half (3.6 TgC yr^{-1}) is evaded from the inland water surface back into the atmosphere and the remainder (3.4 TgC yr^{-1}) flushed out into the Arctic Ocean, proportions in keeping with other, empirically derived studies. (6) DOC exported from the floodplains is dominantly sourced from recent, more 'labile' terrestrial production, in contrast to DOC leached from the rest of the watershed with runoff and drainage, which is mostly sourced from recalcitrant soil and litter. (7) All else equal, both historical climate change (a spring/summer warming of 1.8°C over the catchment) and rising atmospheric CO_2 (+85.6ppm) are diagnosed from factorial simulations to contribute similar, significant increases in DOC transport via primary production, although this similarity may not hold in the future.

Geosci. Model Dev. Discuss., https://doi.org/10.5194/gmd-2018-322
Manuscript under review for journal Geosci. Model Dev.
Discussion started: 25 March 2019

Geoscientific Model Development Discussions

1 Introduction

A new branch of the high latitude-specific land surface component of the IPSL Earth System model, ORCHIDEE MICT-LEAK (r5459), was enabled to simulate new model processes of soil dissolved organic carbon (DOC) and CO_2 production, and their advective/diffusive vertical transport within a discretized soil column as well as their transport and transformation within the inland water network, in addition to improved representation of hydrological and carbon processes in floodplains. These additions, processes first coded in the model ORCHILEAK (Lauerwald et al., 2017) and implemented within the high latitude base model ORCHIDEE-MICT v8.4.1 (Guimberteau et al., 2018), were described in detail in Part 1 of this study. This second part of our study deals with the validation and application of our model. We validate simulation outputs against observation for present-day and run transient simulations over the historial period (1901-2007) using the Lena River basin as test case. The simulation setup and rationale for choice of simulation basin are outlined below.

2 Simulation Rationale

The Lena river basin, which is bounded by the region 52-72°N; 102-142°E, was chosen as the basin for model evaluation because it is the largest DOC discharge contribution amongst the Arctic rivers, according to some estimates (Raymond et al., 2007; Holmes et al., 2012), with its 2.5 million km^2 area (befitting our coarse-grid resolution) discharging almost 20% of the summed discharge of the largest six Arctic rivers, its large areal coverage by Podzols (DeLuca and Boisvenue, 2012), and the dominance of DOC versus particulate organic carbon (POC) with 3-6Tg DOC-C yr^{-1} vs. 0.03-0.04 Tg POC-C yr^{-1} (Semiletov et al., 2011) in the total OC discharge load –factors all broadly representative of the Eurasian Arctic rivers. Compared to other Eurasian rivers, the Lena is relatively well studied, which provides data across the range of soil, hydrologic, geochemical and ecological domains over space and time, that enable us to perform adequate model evaluation.

Climatological forcing is input from the Global Soil Wetness Project Phase 3 (GSWP3) v.0 data at a 1 degree 3-hourly resolution covering the period 1901 to 2007 (Supplement, Table S1), which is then interpolated to a 30 minute timestep to comply with the timestep of the model's surface water and energy balance calculation period. This dataset was chosen for its suitability as input for reproducing the amplitude and seasonality of Northern Hemisphere high latitude riverine discharge in ORCHIDEE-MICT, as compared to other datasets (Guimberteau et al., 2018). An improved floodplains area input file for the Lena basin (Tootchi et al., 2019) was used to drive the simulation of floodplain dynamics (Supplement, Table S1).

Simulations were run over the Lena river basin (Fig. 3a) at a 1 degree resolution (Fig. 1) for the historical period between 1901 and 2007 to evaluate the simulated output of relevant carbon fluxes and hydrologic variables against their observed values, as well as those of emergent phenomena arising from their interplay (Fig. 1), at both the grid and basin scale. We evaluate at the basin scale because the isolation of a single geographic unit allows for a more refined alaysis of simulated variables than doing the same over the global Pan-Arctic, much of which remains poorly accounted for in empirical databases and literature.

Geosci. Model Dev. Discuss., https://doi.org/10.5194/gmd-2018-322
Manuscript under review for journal Geosci. Model Dev.
Discussion started: 25 March 2019

Geoscientific Model Development Discussions

3 Simulation Setup

As detailed in Part 1 (Section 3.1), the soil carbon stock used by our model was reconstituted from the soil carbon spinup of an ORCHIDEE-MICT run from Guimberteau et al. (2018) and run to quasi-steady state equilibrium for the Active and Slow carbon pools (Supplement, Fig. S1) under the new soil carbon scheme used in the model configuration of the present study (Fig. 1). After some adjustment runs to account for different data read/write norms between ORCHIDEE-MICT and this model version, the model was then run in transient mode under historical climate, land cover and atmospheric CO_2 concentrations. A summary of the step-wise procedure for simulation setup described above is detailed graphically in Fig. 1. The model was forced with and run over the climate, CO_2 and vegetation input forcing data for the period spanning 1901-2007 (Supplement, Table S1).

In order to derive an understanding of the environmental drivers of carbon cycling in the Lena watershed and analyze the model sensititivity to the corresponding forcing data, alternative simulations were run with constant climate and CO_2 conditions (Table 1, and Supplement Table S1). Thus a factorial simulation was devised, consisting of 2 factors and 3 simulations whose inputs were otherwise identical but for the investigated factor (Table 1).

4 Results and Discussion

We refer to different simulations performed in this study according to the sensitivity factors to which they are subjected. The 'Control' (CTRL) simulation is that for which transient climate and atmospheric CO_2 forcings are used. CLIM and CO_2 are those simulations for which climate variability and atmospheric CO_2 were held constant at their pre-industriela levels, respectively (Table 1). The following evaluation sections compare observations solely against the CTRL. The subsequent section will evaluate this comparison against the factorial simulations described above.

The overall carbon budgets and their fluxes as generated by each of the simulations are shown in Figs. 2 and 11 and discussed in detail at the end of the evaluation. Below, we examine that budget's component parts, in the following sequential order: In section 4.1 we briefly look through the overall carbon budget of the entire basin, discussing component fluxes of the budget, their values and what they mean. Section 4.2 evaluates DOC discharge, followed by DOC concentrations in export (4.3), dissolved CO_2 transport in rivers and its evasion from the river surface (4.4), emergent phenomena with respect to CO_2 evasion compared to river size (4.5.1) and DOC concentrations and slope (4.5.2), followed by DOC reactivity pools (4.6) and NPP and soil respiration (4.7). Wherever possible, model output are compared with available in situ observations, while emergent relationships between fluxes or concentrations and environmental controls found in observatons are also drawn from the model output, to provide a 'process oriented' evaluation of the model. In Section 4.8 we discuss the overall drivers of the fluxes simulated by our model with respect to the two CLIM and CO_2 factorial simulations and the implications of these for the future.

Geosci. Model Dev. Discuss., https://doi.org/10.5194/gmd-2018-322
Manuscript under review for journal Geosci. Model Dev.
Discussion started: 25 March 2019

4.1 Carbon Budget: Simulated yearly fluxes

Fig. 2 summarises the components of the carbon cycle across the Lena basin, averaged over the decade 1998-2007. All units are in TgC yr^{-1} and the errors are derived from average yearly standard deviations for each of these fluxes. Modelled carbon inputs to terrestrial ecosystems are dominated by photosynthetic input (GPP). GPP assimilates (875 TgC yr^{-1}) are either used as metabolic substrate by plants and lost as CO_2 by plant respiration processes (376 TgC yr^{-1}) or soil respiration processes (465 TgC yr^{-1}), leaving behind annual terrestrial carbon storage in living biomass and soil, known as net biome productivity (NBP, a sink of atmospheric CO_2 of 34 TgC yr^{-1}). Further carbon inputs are delivered to the terrestrial surface via a combination of atmospheric deposition, rainwater dissolved carbon, and the leaching of canopy carbon compounds, all of which summing up to a flux transported to the soil surface (4.6 TgC yr^{-1}) by throughfall (see Part 1, Section 2.5).

In the soil, DOC is produced by the decomposition of litter and soil organic carbon (SOC) pools (see Part 1, Section 2.4 and Fig. 2) and can be ad- or de- sorbed to solid particles (see Part 1, Section 2.11), while there is a continuous exchange of DOC with (solid) soil organic carbon. The interplay between decomposition and sorption leads to DOC concentration changes in the soil solution. DOC in the soil solution as well as a fraction of dissolved CO_2 produced in the root zone from root and microbial respiration is exported to rivers along the model's two hydrological export vectors, surface runoff and deep drainage (Part 1, Section 2.6). For the Lena basin simulations, these fluxes of C exported from soils amount to 5.1 and 0.2 TgC yr^{-1}, for DOC and CO_2 respectively. Three water pools, representing streams, rivers and groundwater and each containing dissolved CO_2 and well as DOC of different reactivity, are routed through the landscape and between grid cells following the river network in the catchment (Part 1, Section 2.7). In addition, seasonally flooded soils located in low, flat grid cells next to the river network (see Part 1, Section 2.8) export DOC (0.57 TgC yr^{-1}) and CO_2 (1.54 TgC yr^{-1}) to the river network when their inundation occurs. Part of this leached inundated material is reinfiltrated back into the soil from the water column during floodplain recession ('Return' flux, 0.45 TgC yr^{-1}). During its transport through inland waters, DOC can be decomposed into CO_2 (2.1 TgC yr^{-1}) and a fraction of river CO_2 produced from DOC and transferred from soil escapes to the atmosphere (3.6TgC yr^{-1}) through gas exhange kinetics (Part 1, Section 2.10). This flux is termed 'CO_2 evasion' in Fig. 2 of this study. Carbon that 'survives' the inland water reactor is exported to the coastal ocean in the form of DOC (3.16 TgC yr^{-1}) and CO_2 (0.26 TgC yr^{-1}). These fluxes and their interpretation within the context of the Land-Ocean-Aquatic Continuum (LOAC) are returned to in Section 4.8 of this study.

4.2 Discharge and DOC flux to the ocean

Simulated river water discharge captures the key feature of Arctic river discharge – that of a massive increase in flow to ~80,000 m^3s^{-1} in April-June caused by melting snow and ice, otherwise known as ice-out or spring freshet, but underestimates observed river discharge in August to October by around 70% which is in the range of ~15,000-28,000 m^3s^{-1} (Figs. 3c, 4b). Given that DOC fluxes are almost directly proportional to river discharge in the Lena basin (Fig. 3d), this sub-optimal performance with regard to hydrology during August to October seeming to be the main cause of a substantial underestimation in simulated bulk DOC outflow. Another cause may simply be the lack

Geosci. Model Dev. Discuss., https://doi.org/10.5194/gmd-2018-322
Manuscript under review for journal Geosci. Model Dev.
Discussion started: 25 March 2019

of peat representation in the model, for which DOC flux concentrations in outflowing fluvial water can be very high (e.g. Frey et al., 2005; 2009: see Section 4.5.1).

In addition, the mean spring (June) discharge peak flows are slightly underestimated or out of phase in simulations (Figs. 3c, 4b) compared to observations (Ye et al., 2009): this is caused by a large amount of water throughput being simulated in May (~10,000 $m^3 s^{-1}$) in excess of observed rates. Finally, during the winter low-flow period, it seems that the model consistently under-estimates water flow-through volumes reaching the river main stem (see Fig. 3c, winter months). Although this underestimate is not severe relative to annual bulk flows, the divergence is large as a percentage of observations (see right-hand axis, Fig. 3c), and may point to an issue in how ice is represented in the model, such as the fact that solid ice inclusions in the soil column are not represented, or the possibility that much slower groundwater dynamics than those represented in the model are feeding discharge.

In addition to this, the presence of a dam on the Vilui tributary of the Lena has been shown to reduce main stem winter low-flow rates by up to 90% (Ye et al., 2003), similar to the discrepancy of our low-flow rates: given that our model only simulates 'natural' hydrological flows and thus does not include dams, we expect that this effect is also at play. Evaluating these considerations, if presently possible, remains beyond the scope of this paper. We note that discharge simulations with ORCHIDEE MICT (Fig. 12 of Guimberteau et al. (2018)) performed with the same climate forcing over the basin are comparable with those from ORCHIDEE MICT-L, with similar overall seasonality and discharge peaks of ~60,000$m^3 s^{-1}$ in the former over the period 1981-2007. This indicates that the modifications made in Bowring et al. (Part 1) focussing on the DOC cycle did not degrade the hydrological performance of the model in this regard.

Our CTRL simulation shows that the yearly sum of DOC output to the Arctic Ocean has increased steadily over course of the 20th Century, from ~1.4Tg DOC-C yr^{-1} in 1901 to ~4Tg DOC-C yr^{-1} in 2007 (Fig. 4a). Smoothing the DOC discharge over a 30-year running mean shows that the increasing trend (Fig. 4a) over this averaging scale is almost linear, at ~0.11TgC per decade, or a net increase of 40% using this averaging scale. Empirically based estimates of total contemporary DOC entering the Laptev Sea from Lena river discharge vary around ~2.5-5.8 TgC-DOC (Cauwet and Sidorov, 1996; Dolman et al., 2012; Holmes et al., 2012; Lara et al., 1998; Raymond et al., 2007; Semiletov et al., 2011).

The red bar in Fig. 4a shows the average simulated DOC discharge of the last decade (1998-2007) of 3.2 TgC yr^{-1}, to be compared with estimates of 3.6 TgC yr^{-1} (black bar) from Lara et al. (1998) and 5.8 TgC yr^{-1} (orange bar) from Raymond et al. (2007) and 5.7 TgC yr^{-1} from Holmes et al. (2012). These estimates are based on different years, different data and different scaling approaches, whose veracity or accuracy are beyond the scope of this study to address or assess.

Nonetheless, the most recent and elaborate of those estimates is that of Holmes et al. (2012) who used a rating curve approach based on 17 samples collected from 2003 to 2006 and covering the full seasonal cycle, which was then applied to 10 years of daily discharge data (1999-2008) for extrapolation. Given that their estimate is also based on Arctic-GRO-1/PARTNERS data (https://www.arcticgreatrivers.org/data), which stands

as the highest temporal resolution dataset to date, we presume that their estimate can be taken to be the most accurate of the actual riverine discharge of DOC from the Lena basin. Compared to their average annual estimate of 5.7 Tg C yr^{-1} then, our simulated DOC export is somewhat low, which can be due to multiple causes:

Firstly, as noted above, the model underestimates observed river discharge. We plot seasonal DOC discharge against river discharge for the Lena outflow grid cell (Kusur station –see Fig. 3a) over 1901-2007 in Fig. 3d, which shows a quasi-linear positive relationship between the two. This dependence is particular to the Arctic rivers, in which the DOC yield of rivers experiences disproportionately large increases in output with increases in discharge yield (Fig. 4, Raymond et al., 2007), relative to the same relationship in e.g. temperate rivers like the Mississippi (Fig. 3, Raymond et al., 2007), owing largely to the 'flushing' out of terrestrially fixed carbon from the previous year's production by the massive runoff generated by ice and snow melt during the spring thaw.

Average river discharge almost doubled between the first and last decades of our simulation (Fig 4c), giving further credence to the relationship between DOC and water discharge. Comparing simulated annual mean discharge rate (m^3 s^{-1}) with long-term observations (Ye et al. 2003) over years 1940-2000 (Fig. 4c) shows that though absolute discharge rates are underestimated by simulations, their interannual variation reasonably tracks the direction and magnitude of observations. Linear regressions through each trend yield very similar yearly increases of 29 vs 38 m^3 s^{-1} yr^{-1} for simulations and observations, respectively, while the mean annual water discharge differential hovers at 30% (Fig. 4c), a fraction similar to that of the simulated and observed (Raymond et al., 2007; Holmes et al., 2012) bulk annual DOC discharge discrepancy (Fig. 4a).

Figure 4b plots discharge over the first (1901-1910) and last (1998-2007) decades of simulated monthly DOC and river discharge with observed river discharge. The bulk of the DOC outflow occurs during the spring freshet or snow/ice-melting period of increased discharge, accounting for ~50-70% of the year's total Lena outflow to the Arctic (Lammers et al., 2001; Ye et al., 2009), with peak river discharge rates in June of ~80,000 m^3 s^{-1}. DOC concentrations increase immensely at this time, as meltwater flushes out DOC accumulated from the previous year's litter and SOC generation (Raymond et al., 2007; Kutscher et al., 2017).

This is reproduced in our simulations given that DOC discharge peak occurs at the onset of the growing season, meaning that outflow DOC is generated from a temporally prior stock of organic carbon. Simulation of the hydrological dynamic is presented in maps of river discharge through the basin in Fig. 3b, which show low-flows in April with substantial hydrographic flow from upstream mountainous headwaters and Lake Baikal inflow in the south, peak flow in June with substantial headwater input in the northern portion and a moderate flow through the mainstem with little headwater input in September.

In Fig. 4b we observe that (i) DOC discharge fluxes closely track hydrological fluxes (solid versus dashed lines); (ii) the simulated modern river discharge peak is very close to the historical observed discharge peak, however it slightly overestimates spring

fluxes and substantially underestimates fluxes in the Autumn (dashed red versus black lines). Thus the discrepancy between simulated bulk DOC discharge fluxes and empirical estimates may largely be found in the simulated hydrology. (iii) The curve shape of discharge fluxes differs greatly between the first and last decades of simulation.

The difference between the first and last decades of the simulation in Fig. 4b is mostly attributable to a large increase in the DOC flux mobilised by spring freshet waters that culminate in the early summer outflow of DOC to the ocean, which generate the peaks in DOC flux. This suggests both greater peaks in simulated DOC flux and a shift to earlier peak timing, owing to an increase in river discharge indicative of an earlier spring and a progressively warmer environment. (iv) The maximum modeled modern monthly DOC flux rate of ~1.3 TgC month^{-1} (Fig. 4b, solid red line) is comparable to the mean maximum DOC flux rate measured in a recent study, which showed that the aggregate carbon discharge flux of the Lena River over its 2-month peak period in 2013 was 3.5 TgC, giving a mean flux of 1.75 TgC month^{-1} (Kutscher et al., 2017, Fig. 2).

The monthly pattern of DOC discharge approximates the seasonal pattern found in an empirical Pan-Arctic DOC discharge study by Raymond et al. (2007), which they take to represent total Lena river DOC discharge. The latter study, which looks at Pan-Arctic DOC discharge rates, finding them to be 15-20% higher than in prior estimates, gives discharge maxima in May, whereas our simulated maxima are in June. We compare the Raymond et al. (2007) modern DOC outflow (Fig. 4d, solid black line) from the Lena river at Zhigansk (Raymond et al., 2007) against simulated DOC outflow from the Zhigansk site as well as from the river outflow site (Kusur) 500km downstream (Fig. 4d, solid blue and solid red lines, respectively).

Simulated DOC flux is underestimated for both sites. Peakflow at Zhigansk seems to be attenuated over May and June in simulations, as opposed to May peakflow in observations, while peakflow at Kusur is definitively in June. This suggests that simulated outflow timing at Zhigansk may slightly delayed, causing a split in peak discharge when averaged in the model output. Thus the aggregation of model output to monthly averages from calculated daily and 30 minute timesteps can result in the artificial imposition of a normative temporal boundary (i.e. month) on a continuous series. This may cause the less distinctive 'sharp' peak seen in Fig. 4d, ,which is instead simulated at the downstream Kusur site, whose distance some 500km away from Zhigansk more clearly explains the delay difference in seasonality.

We further evaluate our DOC discharge at the sub-basin scale, to see if the simulated aggregate flux exiting the Lena river mouth is composed of a coarsely realistic breakdown of source matter geography. In other words, whether the fractional contribution of different DOC flows from rivers draining the simulated Lena basin correspond to those in the observed basin. This comparison is depicted in Fig. 5, where, again using data from Kutscher et al., (2017), the observed and simulated percentage DOC contributions of the Aldan, Vilui, and Upper and Lower Lena sub-basins to total flux rates are 19 (24)%, 20(10%), 33 (38%) and 30 (28)% in simulations (observations) for the four basins, respectively.

While deviations between simulation and observation can be expected given the difference in magnitude and timing of DOC discharge previously discussed, in addition to interannual variability, the nearly twofold value mismatch of the Vilui basin likely has its roots in the fact in its real-word damming, not represented here. On the other hand, we cannot explain the ~5% discrepancies in other sub-basin fluxes, particularly for the Aldan.

Of the shortcomings in our model with respect to observations, year-on-year variations over the decade 1998-2007 may be of significance, given that the Holmes et al. (2012) and Raymond et al. (2007) DOC discharge values are significantly higher than total organic carbon (DOC+POC) outflow estimates (~5.0-5.4 TgC yr^{-1}, Fig. 4a blue boundary) as presented in Lara et al. (1998). To this we can add scale-related inaccuracies in the routing protocol that can lead to small geographic inconsistencies in simulated versus observed phenomena, as well as the exclusion of explicit peatland formation and related dynamics in this model, which is the subject of further model developments within the ORCHIDEE-MICT envelope (Qiu et al., 2018) that have yet to be included in this iteration. With peatlands thought to cover ~17% of the Arctic land surface (Tarnocai et al., 2009), and with substantially higher leaching concentrations, this may be a significant omission from our model's representation of high latitude DOC dynamics.

4.3 DOC Concentrations in lateral transport

The range of simulated riverine DOC concentrations approximates those found in the literature for the Lena and other Eurasian high-latitude river basins (e.g. Arctic-GRO 1 (https://www.arcticgreatrivers.org/data); Denfeld et al., 2013; Mann et al., 2015; Raymond et al., 2007; Semiletov et al., 2011). In those for the Lena, observed average DOC concentrations hover at ~10mgC L^{-1}. Likewise, simulated DOC concentrations mostly lie in the range of 0-10 mgC L^{-1}, with monthly grid cell maxima of 1-200 mgC L^{-1}, and on flow-weighted average exhibit the observed seasonal range and amplitude. Figure 6 summarises some of this simulated output, showing maps of mean monthly DOC concentration for stream water, river water and groundwater (Fig. 6a,b,c, respectively) in April, June and September –the beginning, middle and end of the non-frozen period in the basin, respectively, over 1998-2007.

For both the stream and river water reservoirs, DOC concentrations appear to have spatio-temporal gradients correlated with the flux of water over the basin during the thaw period, with high concentrations of 10-15 mgC L^{-1} as the snow and ice melts in April in the upstream portions of the basin, these high concentrations moving northward to the coldest downstream regions of the basin in June. Lower DOC concentrations of ~5 mgC L^{-1} dominate the basin in September when the bulk of simulated lateral flux of DOC has dissipated into the Laptev Sea, bearing in mind that we underestimate the river discharge flux in the Autumn. In contrast, groundwater DOC concentrations are generally stable with time, although some pixels appear to experience some 'recharge' in their concentrations during the first two of the three displayed thaw months. Significantly, highest groundwater DOC concentrations of up to 20 mgC L^{-1} are focussed on the highest elevation areas of the Lena basin on its Eastern boundary, which are characterized by a dominance of Podzols (SI, Fig. 2b).

This region, the Verkhoyansk range, is clearly visible as the high groundwater DOC

Geosci. Model Dev. Discuss., https://doi.org/10.5194/gmd-2018-322
Manuscript under review for journal Geosci. Model Dev.
Discussion started: 25 March 2019

concentration(2-20mgC L^{-1}) arc (in red) in Fig. 6a, as well as other high elevation areas in the south-western portion of the basin (see Fig. 3a for the basin grid cell mean topographic slope), while the central basin of very low mean topographic slope exhibits much smaller groundwater DOC concentrations (0-2mgC L^{-1}). The range of simulated groundwater DOC concentration comes close to those aggregated from the empirical literature by Shvartsev (2008) in his seminal review of global groundwater geochemistry, which finds from >9000 observations that groundwater in permafrost regions exhibit a mean concentration of ~10 mgC L^{-1} after peatlands and swamps (not simulated here) are removed (Table 2).

The high groundwater reservoir DOC concentrations simulated in high altitude regions by ORCHIDEE MICT-L is related to the fact that, in the model, DOC is rapidly produced and infiltrated deep into soil above the permafrost table, to the point that it reaches the simulated groundwater pool relatively quickly, allowing it to enter this reservoir before being metabolised through the soil column –hence allowing for the relatively high groundwater concentrations found in mountain areas. Because of the prevailing low temperatures, this DOC is not quickly decomposed by microbes and instead feed the groundwater DOC pool.

4.4 In-Stream CO_2 Production, Transport, Evasion

In our model, the fate of DOC once it enters the fluvial system is either to remain as DOC and be exported to the ocean, or to be degraded to dissolved CO_2 ($CO_{2(aq.)}$), which is itself either also transported to the marine system or outgassed from the fluvial surface to the atmosphere (see Part 1, Section 2.10). The latter two outcomes also apply to $CO_{2(aq.)}$ produced in the soil by organic matter degradation and subsequently transported by runoff and drainage flows to the water column. As shown in Fig. 2, a large proportion of DOC (38%, 2.1 TgC yr^{-1}) that enters the water column is degraded to $CO_{2(aq.)}$ during transport, which adds to the 1.65 TgC yr^{-1} of direct $CO_{2(aq.)}$ input from the terrestrial land surface. Of this bulk CO_2 exported into and generated within the water column, 3.6 TgC yr^{-1} evades from the water surface to the atmosphere before reaching the river delta. In what follows, we evaluate first inputs of $CO_{2(aq.)}$ to the water column in terms of their seasonality, before evaluating CO_2 evasion rates and the relation of this to smaller and larger water bodies (river versus stream).

The seasonality of riverine dissolved CO_2 concentrations ($CO_{2(aq.)}$, mgC L^{-1}) is evaluated in Fig. 4d to compare $CO_{2(aq.)}$ concentrations with DOC bulk flows, since $CO_{2(aq.)}$ concentrations follow an inverse seasonal pattern to those of DOC, being highest during the winter baseflow period and lowest in summer due to dilution during its high discharge phase (Semiletov et al., 2011). The simulated flow of $CO_{2(aq.)}$ at Kusur (Fig. 4d, dashed red) reproduces the seasonality of observations from Cauwet and Sidorov (1996), who sampled the Lower Lena (ship-board, several sites in river delta region (see Fig. 3a)), but somewhat underestimates concentrations, this perhaps due to the absence of peat representation in our model, in combination with underestimated hydrological discharge. Also included in Fig. 4d is the basin average for all non-zero values, whose shape also tracks that of observations. Thus the model represents on the one hand increasing hydrological flow mobilising increasing quantities and concentrations of DOC while on the other hand those same increasing hydrological flows increasing the flux, but decreasing the concentration, of $CO_{2(aq.)}$ throughput.

To our knowledge, no direct measurements for CO_2 evasion from the surface of the Lena river are available in the literature, presumably owing to the notorious difficulty in successfully obtaining such data. We refer to Denfeld et al. (2013) for evaluating our evasion flux results, since their basin of study, the Kolyma River, is the most geographically proximate existing dataset to the Lena, despite biogeographical differences between the two basins –namely that the Kolyma is almost entirely underlain by continuous permafrost. The Kolyma River CO_2 evasion study measured evasion at 29 different sites along the river basin (~158-163°E; 68-69.5°N), with these sites distinguished from one another as 'main stem', 'inflowing river' or 'stream' on the basis of reach length. The study showed that during the summer low-flow period (August), areal river mainstem CO_2 evasion fluxes were ~0.35 gC m^{-2} d^{-1}, whereas for streams of stream order 1-3 (widths 1-19m), evasion fluxes were up to ~7 gC m^{-2} d^{-1}, and for non-mainstem rivers (widths 20-400m) mean net fluxes were roughly zero (Table 3 of Denfeld et al., 2013). Thus, while small streams have been observed to contribute to roughly 2% of the Kolyma basin surface area, their measured percentage contribution to total basin-wide CO_2 evasion ~40%, whereas for the main stem the surface area and evasion fractions were ~80% and 60%, respectively.

Results such as these, in addition to permafrost soil incubation experiments (e.g. Drake et al., 2015; Vonk et al., 2013, 2015b, 2015a) suggest that small streams, which represent the initial (headwater) drainage sites of these basins, rapidly process hydrologically leached carbon to the atmosphere, and that this high-reactivity carbon is a mix of recently thawed ancient permafrost material, as well as decomposing matter from the previous growth year. This is given as evidence that the total carbon processing of high-latitude rivers is significantly underestimated if only mainstem carbon concentrations are used in the accounting framework, since a large amount of carbon is metabolised to the atmosphere before reaching the site of measurement.

Figure 7 summarises some of the results from the simulated water body CO_2 outgassing flux. Year-on-year variation in basin-wide evasion from river, stream and floodplain sources combined exhibits a marked increasing trend over the course of the 20th Century, increasing from a minimum of ~1.6 $TgCO_2$-C yr^{-1} in 1901 to a maximum of ~4.4 $TgCO_2$-C yr^{-1} in 2007, an increase of almost 300% (Fig. 7a). Smoothing the data over a 30 year running average yields a dampened net increase in basin-wide evasion of ~30% over the historical period on this averaging scale (Fig. 7a). Thus yearly evasion flux is some 105% of yearly DOC discharge to the coast from the Lena basin and 51% of C exported from soils to headwaters as CO_2 or DOC. If we compare the mean yearly rate of increase in absolute (TgC yr^{-1}) CO_2 evasion and DOC discharge based on linear regression over the whole simulation period, it appears that the rate of increase of both fluxes has been strikingly similar over the simulated 20th Century, with mean increases of 11.1 GgC yr^{-1} and 11.5 GgC yr^{-1} per year for evasion and export, respectively.

The heterogeneity of CO_2 evasion from different sources in the model is most evident in terms of their geographic distribution and relative intensity, as shown in the evasion flux rate maps (tons grid $cell^{-1}$ d^{-1}) over floodplain, stream and river areas in April, June and September (Fig. 8a-c). Whereas floodplains (Fig. 8a) tend to have some of the highest evasion rates in the basin, their limited geographic extent means that their contribution to basinwide evasion is limited for the whole Lena. Stream evasion

Geosci. Model Dev. Discuss., https://doi.org/10.5194/gmd-2018-322
Manuscript under review for journal Geosci. Model Dev.
Discussion started: 25 March 2019

meanwhile (Fig.8b), tends to be broadly distributed over the whole basin, representing the fact that small streams and their evasion are the main hydrologic connectors outside of the main river and tributary grid cells, whereas river evasion (Fig. 8c) is clearly linked to the hydrographic representation of the Lena main stem itself, with higher total quantities in some individual grid cells than for the stream reservoir, yet distributed amongst a substantially smaller number of grid cells. Whereas the stream reservoir has greatest absolute evasion flux rates earlier in the year (April-May), maximum evasion rates occur later in the year and further downstream for the river reservoir, reflecting the fact that headwaters are first-order integrators of soil-water carbon connectivity, whereas the river mainstem and tributaries are of a secondary order. Note that the September values must be interpreted with caution, given the underestimation in our simulations of the river discharge during the Autumn period.

The spatio-temporal pattern of increasing evasion over the simulation period is shown in Fig. 7b as a Hovmöller difference plot, between the last and first decade, of log-scale average monthly evasion rates per latitudinal band. This shows that the vast majority of outgassing increase occurs between March and June, corresponding to the progressive onset of the thaw period moving northwards over this timespan. Although relatively small, outgassing increases are apparent for most of the year, particularly at lower latitudes. This would suggest that the change is driven most acutely by relatively greater temperature increases at higher latitudes ('Arctic amplification' of climate warming, e.g. Bekryaev et al., 2010) while less acute but more temporally homogenous evasion is driven by seasonal warming at lower latitudes.

As previously discussed, the proportion of total basin-wide CO_2 evasion attributable to headwater streams and rivers is substantially greater than their proportion of total basin surface area. Figure 7c represents the mean monthly fractional contribution of each surface hydrological water pool to the total evasion flux (unitless) over the period 1998-2007. This shows that over the entirety of the thaw period, the stream water pool takes over from the river water pool as the dominant evasion source, particularly at the height of the freshet period, where its fractional contribution rises to >75%.

The stream fraction of August outgassing is roughly 57% of the annual total, which is higher than the ~40% found for streams in the Denfeld et al. (2013) study. However, the values between the two studies are not directly comparable, different basins notwithstanding. This is because in ORCHIDEE MICT-L, the 'stream' water reservoir is water routed to the river network for all hydrologic flows calculated to not cross a 0.5 degree grid cell boundary (the resolution of the routing module, explained in Part 1, Section 2.6), which may not be commensurate with long, <20m wideth streams in the real-world, that were used in the Denfeld et al. (2013) study. In addition, this 'stream' water reservoir in the model does not include any values for width or area in the model, so we cannot directly compare our stream reservoir to the <20m width criterion employed by Denfeld et al. (2013) in their definition of an observed stream. Thus our 'stream' water reservoir encompasses substantially greater surface area and hydrologic throughput than that in the Denfeld et al. study. We also add the qualification that because of its coarse-scale routing scheme, ORCHIDEE isn't able to simulate stream orders lower than 4 or 5 thus missing a potentially substantial vector for the water-surface evasion of CO_2.

Significantly, also shown in Fig. 7c, is the gradual onset of evasion from the floodplain reservoir in April, as the meltwater driven surge in river outflow leads to soil inundation and the gradual increase of proportional evasion from these flooded areas over the course of the summer, with peaks in June-August as water temperatures over these flooded areas likewise peak. We stress the importance of these simulation results as they concur with large numbers of observational studies (cited above) which show smaller headwater streams' disproportionately large contribution to total outgassing (Fig. 7c), this being due to their comparatively high outgassing rates (Fig. 7e). In addition, the contribution of floodplains to evasion, an otherwise rarely studied feature of high latitude biomes, is shown here to be significant.

A Hovmöller plot (Fig. 7d) of the monthly longitude-averaged stream reservoir fraction of total evasion, gives some indication as to the spatio-temporal pattern under which evasion from this hydrological pool evolves over the course of the year. From this we can infer that: (i) The dominance of stream evasion begins in the most southern upstream headwaters in the lower latitude thaw period (April-May), and trickles northward over the course of the next two months, following the riverflow. (ii) The intensity of stream water evasion is greatest in the lower latitude regions of the basin, which we speculate is the result of higher temperatures causing a greater proliferation of small thaw water-driven flows and evasion. (iii) Areas where the stream fraction is not dominant or only briefly dominant during the summer (58-60°N, 63-64°N, 70-71°N) are all areas where floodplain CO_2 evasion plays a prominent role at that latitudinal band.

Although not directly comparable due to the previously mentioned issues arising from our model-derived representation of 'stream' water versus those in the real world, we evaluate the approximate rate of areal CO_2 efflux from the water surface against obervations from Denfeld et al. (2013). The 'approximate' caveat refers to the fact that model output doesn't define a precise surface area for the stream water reservoir, which is instead bundled into a single value representing the riverine fraction of a grid cell's total surface area. Thus, in order to break down the areal outgassing for the stream versus river water reservoirs, we derive an approximate value for the fractional area taken up by rivers and streams in a simple manner: we weight the total non-floodplain inundated area of each grid cell by the relative total water mass of each of the two hydrological pools, then divide the total daily CO_2 flux simulated by the model by this value. The per-pool areal estimate is an approximation since it assumes that rivers and streams have the same surface area: volume relationship. This is clearly not the case, since streams are generally shallow, tending to have greater surface area per increment increase in depth than rivers. Thus, our areal approximations are likely underestimated (overestimated) for streams (rivers), respectively.

The comparison of simulated results with those from Denfeld et al. (2013) are displayed in Fig. 7e, which shows boxplots for simulated CO_2 evasion (gC m^{-2} d^{-1}) from the stream water reservoir and river water reservoir averaged over 1998-2007. The empirical (Kolyma river) analog of this data, from which this plot is inspired (Fig. 4d in Denfeld et al., 2013), is shown inset in the figure, with whiskers in their case denoting measured maxima and minima. Median efflux was 1.1 (6) versus 0.4 (0.8) for stream and river, respectively, in simulations (observations). Like the observations, simulated stream efflux had a substantially greater interquartile range, mean (24.6) and standard

Geosci. Model Dev. Discuss., https://doi.org/10.5194/gmd-2018-322
Manuscript under review for journal Geosci. Model Dev.
Discussion started: 25 March 2019

deviation (73) than total river efflux (1.3 and 7.2, respectively). Note that from ~700 non-zero simulation datapoints, 7 were omitted as 'outliers' from the stream reservoir efflux statistics described below, because very low stream:river reservoir values skewed the estimation of total approximate stream surface area values very low, leading to extreme efflux rate values of 1-3000gC m^{-2} d^{-1} and are thus considered numerical artefacts of the areal approximation approach used here.

4.5 Emergent Phenomena

4.5.1 DOC and mean annual air temperature

A key emergent property of DOC concentrations in soils and inland waters should be their positive partial determination by the temperature of the environment under which their rates of production occur, as has been shown in the literature on permafrost regions, most notably in Frey & Smith (2005) and Frey & McClelland (2009).

Increasing temperatures should lead to greater primary production, thaw, decomposition and microbial mobilisation rates, and hence DOC production rates, leading to (dilution effects notwithstanding) higher concentrations of DOC in thaw and so stream waters. Looking at this emergent property allows us to evaluate the soil-level production of both DOC and thaw water at the appropriate biogeographic and temporal scale in our model. This provides a further constraint on model effectiveness at simulating existing phenomena at greater process-resolution.

Figure 9 compares three datasets (simulated and two observational) of riverine DOC concentration (in mgC L^{-1}) plotted against mean annual air temperature (MAAT). The simulated grid-scale DOC versus MAAT averaged over July and August (for comparability of DOC with observational sampling period) of 1998-2007 is shown in red, and observed data compiled by Laudon et al. (2012) and Frey and Smith (2005) for sites in temperate/cold regions globally and peatland-dominated Western Siberia, respectively. The Laudon et al. (2012) data are taken from 49 observations including MAAT over the period 1997-2011 from catchments north of 43°N, and aggregated to 10 regional biogeographies, along with datapoints from their own sampling; those in the Frey and Smith study are from 55-68°N and ~65-85°E (for site locations, see Laudon et al. (2012), Table 1 and 2; Frey and Smith (2005), Fig. 1).

Fig. 9 can be interpreted in a number of ways. First, this MAAT continuum spans the range of areas that are both highly and moderately permafrost affected and permafrost free (Fig. 9, blue and green versus orange shading, respectively), potentially allowing us a glimpse of the behaviour of DOC concentration as the environment transitions from the former to the latter. Simulated Lena DOC concentrations, all in pixels with MAAT < -2°C and hence all bearing continuous or discontinuous permafrost ('permafrost-affected' in the figure), only exhibit a weakly positive response to MAAT on the scale used ($y=6.05e^{0.03MAAT}$), although the consistent increase in DOC minima with MAAT is clearly visible.

Second, the Laudon et al. (2012) data exhibit an increasing then decreasing trend over the range of MAAT (-2°C to 10°C) in their dataset, which they propose reflects an 'optimal' MAAT range for the production and transport of DOC, occupying the 0°C to 3°C range (Fig. 9, red shading). Below this optimum range, DOC concentrations may be

Geosci. Model Dev. Discuss., https://doi.org/10.5194/gmd-2018-322
Manuscript under review for journal Geosci. Model Dev.
Discussion started: 25 March 2019

limited by transport due to freezing, and above this, smaller soil carbon pools and temperature-driven decomposition would suppress the amount of DOC within rivers. Third, the lower end of the Laudon et al. (2012) MAAT values correspond to a DOC concentration roughly in line with DOC concentrations simulated by our model at those temperatures.

Fourth, DOC concentrations in the Frey and Smith (2005) data exhibit a broad scattering in permafrost-affected sites, with concentrations overlapping those of our simulations (Fig. 9, green shading), before rapidly increasing to very high concentrations relative to the Laudon et al. (2012) data, as sites transition to permafrost-free (red shading, $y=3.6_{MAAT}+29.4$). Their data highlight the difference in DOC concentration regime between areas of high (Frey and Smith, 2005) and low (Laudon et al., 2012) peatland coverage and the different response of these to temperature changes. Fifth, because our simulation results largely correspond with the observed data where the MAAT ranges overlap (green shading), and because our model does not include peatland specific processes, we should expect our model to broadly follow the polynomial regression plotted for the Laudon et al. (2012) data as temperature inputs to the model increase. Figure 9 implies that this increase should be on the order of a doubling of DOC concentration as a system evolves from a MAAT of -2°C to 2°C. In addition, as the Arctic environment warms we should expect the response of DOC concentrations as a whole to reflect a mix of both observationally-derived curves, as a function of peatland coverage.

4.5.2 DOC and topographic slope

Subsurface water infiltration fluxes and transformations of dissolved matter represent an important, if poorly understood and observationally under-represented biogeochemical pathway of DOC export to river main stems, involving the complex interplay of slope, parent material, temperature, permafrost material age and soil physical-chemical processes, such as adsorption and priming.

In the Lena basin, as in other permafrost catchments, topographic slope has been shown to be a powerful predictor for water infiltration depth, and concentration and age of dissolved organic carbon (Jasechko et al., 2016; Kutscher et al., 2017; McGuire et al., 2005), with deeper flow paths and older, lower DOC-concentrated waters found as the topographic slope increases. This relationship was shown in Fig. 4 of Kutscher et al. (2017) who surveyed DOC concentrations across a broad range of slope angle values in the Lena basin and found a distinct negative relationship between the two. We compare the Kutscher et al. (2017) values with our model output, by plotting stream and river DOC concentrations averaged per gridpoint over 1998-2007 against the topographic map used in the routing scheme, versus their empirically derived data (Fig. 10). As shown therein, a similar negative relationship between the two variables is clearly apparent.

A similar relationship was found in temperate rivers by Lauerwald et al. (2012), and a recent paper by Connolly et al. (2018), based on their observational data and a synthesis of Pan-Arctic empirical literature. They showed that for Arctic catchments in general, the relationship of DOC concentration in fluvial waters scaled in a consistent and strongly negative manner against topographic slope. This was found for all Arctic catchments, globally, prompting Connolly et al. to argue that topographic slope may be a type of

'master variable' for estimating fluvial DOC concentrations in the absence of viable *in* situ measurement programs.

The reasoning for the negative slope-DOC concentration relationship is that as elevation increases, temperature and primary production decreases. This leads to a thinner organic soil layer, meaning that mineral soil plays a stronger role in shallow hydrologic flowpaths, allowing for deeper infiltration and shorter residence time in a given soil layer. In addition, steeper terrain leads to a lower soil water residence time and lower moisture than in flat areas.

As a result, a given patch of soil matter will be exposed to leaching for less (residence) time, while the organic matter that is leached is thought to be adsorbed more readily to mineral soil particles, leading to either their re-stabilisation in the soil column or shallow retention and subsequent heterotrophic respiration in situ, cumulatively resulting in lower DOC concentrations in the hydrologic export (Kaiser and Kalbitz, 2012; Klaminder et al., 2011). This line of reasoning was recently shown to apply also to deep organic permafrost soils (Zhang et al., 2017), although the degree to which this is the case in comparison to mineral soils is as yet unknown.

In addition, and as described in Part 1 (Section 2.5) of this study, MICT-L contains a provision for increased soil column infiltration and lower decomposition rates in areas underlain by Podzols and Arenosols. The map from the Harmonized World Soil Database (Nachtergaele, 2010), which is used as the input to this criterion, shows areas underlain by these soils in the Lena basin to also be co-incident with areas of high topographic slope (Fig. 3a, SI, Fig S2b). Their Podzol effect is to increase the rate of decomposition and infiltration of DOC, relative to all other soil types, thus also increasing the rate of DOC flux into groundwater (see Part 1 of this study, Section 2.5).

Our modelling framework explicitly resolves the processes involved in these documented dynamics –soil thermodynamics, solid vertical flow (turbation), infiltration as a function of soil textures and types, adsorption as a function of soil parameters (see Part 1 of this study, Section 2.11), DOC respiration as a function of soil temperature and hence depth (Part 1, Section 2.12), lagging of DOC vertical flow behind hydrological drainage flow (summary Figure in Part 1, Fig. 1). We thus have some confidence in reporting that the simulated negative relationship of DOC concentration with topographic slope may indeed emerge from the model. If generalisable to permafrost basins as a whole, this relationship may be an emergent process-based signal with which to evaluate the biogeographic performance of permafrost-region DOC modelling initiatives in the future, as was recently suggested by Connolly et al. (2018).

4.6 DOC Reactivity Pools

Here we examine the reactivity of DOC leached from the soil and litter to different hydrological export pools. Surface runoff DOC export is dominated by refractory carbon (Fig. 11a), with export rates largely following discharge rates as they drain the basin with an increasing delay when latitude increases. As the thaw period gets underway (April), the fraction of labile carbon in surface runoff DOC increases substantially from south to north, reflecting the hydrologic uptake of the previous year's undecomposed high-reactivity organic matter, as well as the addition of new inputs from the onset of

734 the current year's growing season.
735
736 Refractory carbon–dominated drainage DOC export rates (Fig. 11a) are centered on the
737 months June through October, with refractory export rate intensities per latitudinal
738 band during this period largely consistent with the fraction of inundated area (Fig. S1)
739 experienced by these bands during the course of the year, these centering on the areas
740 bounded by 52-65N and 70-72N. The high refractory proportion of drainage flow is
741 expected, as drainage leaches older, relict soil and litter matter. Because of its longer
742 water residence time, labile DOC carried vertically downward through the soil
743 infiltration flux will tend to be metabolised in situ before it can be exported to the
744 hydrological network, thus further increasing the proportion of refractory carbon.
745
746 By contrast floodplain DOC export (Fig. 11a) is dominated by the labile carbon pool but
747 is composed of more nuanced mix of both reactivity classes, reflecting its relatively
748 greater dependence on the current year's 'fresh' biomass as source material (62% labile
749 DOC versus 38% refractory DOC, year-averaged) for carbon leaching. This can be
750 expected, since DOC and CO_2 production that would normally occur first in soil free DOC
751 concentrations before being gradually exported into surface runoff and drainage inputs
752 to the hydrological network are instead directly supplied to the water column as they
753 are generated, meaning that there is less of a time lag for the rapid decomposition of the
754 labile portion than through the other two hydrological export pathways.
755
756 For both the river and stream pool, mean DOC concentrations are also dominated by
757 refractory carbon sources. Interestingly, very high concentrations in the stream
758 reservoir are maintained year-round in the northernmost reaches of the Lena basin, the
759 causes of which are not directly deducible from our data. Likely, very high stream
760 concentrations are obtained from the confluence of relatively low volumetric water
761 fluxes in these regions that owe themselves to the freezing temperatures, with these low
762 temperatures likewise retarding direct heterotrophic respiration of contemporary plant
763 litter and favouring instead their environmental mobilisation by hydrological leaching,
764 when liquid water is available for matter dissolution.
765
766 When averaged over the year, the dominance of the refractory DOC carbon pool over its
767 labile counterpart is also evident for all DOC inputs to the hydrological routing except
768 for floodplain inputs, as well as within the 'flowing' stream and river pools themselves.
769 This is shown in Table 2, where the year-averaged percentage of each carbon
770 component of the total input or reservoir is subdivided between the 'North' and 'South'
771 of the basin, these splits being arbitrarily imposed as the latitudinal mid-point of the
772 basin itself (63N). This reinforces the generalised finding from our simulations that
773 refractory carbon dominates runoff and drainage inflows to rivers (89% refractory, on
774 average), while floodplains export mostly labile DOC to the basin (64%), these values
775 being effectively independent of this latitudinal sub-division (Table 2). This may be
776 expected, given that almost the entire basin is underlain by continuous permafrost,
777 whereas in areas with discontinuous or sporadic permafrost, the combination of higher
778 primary productivity and so litter input, with seasonal thaw of labile permafrost soil
779 matter may be expected to substantially increase the labile portion of the overall sum of
780 these quantities. Nonetheless, there appears to be a small consistent difference between
781 North and South in the stream and river water DOC makeup, in that the labile portion
782 decreases between North and South ; this may be an attenuated reflection of the portion

Geosci. Model Dev. Discuss., https://doi.org/10.5194/gmd-2018-322
Manuscript under review for journal Geosci. Model Dev.
Discussion started: 25 March 2019

of labile DOC that is decomposed to CO_2 within the water column during its transport northward, affecting the bulk average proportions contained within the water in each 'hemisphere'.

4.7 NPP and Soil Respiration

Rates of yearly net primary production (NPP) for Russian and Siberian forests have been inferred in situ from eddy flux and inventory techniques to range from 123-250 gC m^{-2} yr^{-1} (Beer et al., 2006; Lloyd et al., 2002; Roser et al., 2002; Schulze et al., 1999; Shvidenko and Nilsson, 2003). We likewise simulate a broad range of NPP carbon uptake rates, of 61-469 gC m^{-2} yr^{-1} averaged per grid cell over the Lena basin, with a mean value of 210 gC m^{-2} yr^{-1}. NPP is heterogeneously distributed over space and between PFTs (SI, Fig. S4c), with forests averaging 90 gC m^{-2} yr^{-1} and grasslands averaging 104 gC m^{-2} yr^{-1} over the basin as a whole. Low values tended to originate in basin grid cells with elevated topography or high mean slope, while the maximum value was standalone, exceeding the next greatest by ~100 gC m^{-2} yr^{-1}, and is most likely caused by the edge effects of upscaling a coastal gridcell's small fraction of terrestrial area where high productivity occurs in a small plot, to the grid cell as a whole. By evaluating NPP we are also evaluating at a secondary level litter production, which is at a third level a major component of DOC production.

Taken as a whole, gross primary production (GPP) was performed under simulations by four PFT groups, with the largest basin-wide bulk contributions coming from boreal needleleaf summer-green trees and C3 grasses (SI, Fig. S4a), the highest GPP uptake rates (3 TgC $pixel^{-1}$ yr^{-1}) generated by boreal needleleaf evergreen trees, and the remainder of GPP contributed by Boreal broad-leaved summer-green trees (SI, Fig. S4a).

Soil respiration rates, of combined soil heterotroph and plant root respiration in our Control simulation, averaged 208 gC m^{-2} yr^{-1} (0.57 gC m^{-2} d^{-1}) over the Lena basin over the period 1990-2000, which is somewhat higher than those found by Elberling (2007) in forest soils over Svalbard, of 103-176 gC m^{-2} yr^{-1} (0.28-0.48 gC m^{-2} d^{-1}). Sawamoto, et al. (2000) measured in situ summertime soil respiration over the central Lena basin and found rates of 1.6-34 gC m^{-2} d^{-1}, while Sommerkorn (2008) observed rates of 0.1-3.9 gC m^{-2} d^{-1} at higher latitudes, these appearing to vary with vegetation and fire history, water table depth and temperature. Mean heterotrophic respiration rates of 1.6 gC m^{-2} d^{-1} are simulated here during July and August, in the range 0.0.5-2.2 gC m^{-2} d^{-1} for each of the above PFT groups. The spatial distribution of, and difference in respiration rates between PFT groups largely mirrors those for NPP (SI Fig. S4c), with maximum rates of 1.4 gC m^2 d^{-1} over forested sites, versus a maximum of 2.2 gC m^2 d^{-1} over grassland/tundra sites (SI, Fig. S4b).

Aggregated over the basin, results show that increases over the course of the 20th Century were simulated for NPP, GPP, River Discharge, DOC, $CO_{2(aq.)}$, autotrophic and heterotrophic respiration and CO_2 evasion, with percentage changes in the last versus first decade of +25%, +27%, 38%, +73%, +60%, +30%, +33% and +63%, respectively. (Fig. 11b). It thus appears that rising temperatures and CO_2 concentrations disproportionately favoured the metabolisation of carbon within the soil and its transport and mineralisation within the water column, fed by higher rates of primary production and litter formation as well as an accelerated hydrological cycle (see Fig. 4b

and 13a).

In Figure 11c we run linear regressions through scatter-plots of yearly DOC and CO_2 export and CO_2 evasion fluxes, versus rates of NPP (TgC yr^{-1}). These show that whereas bulk DOC flux appears most sensitive (steeper slope) to increases in NPP, it is also least coupled to it (more scattered, R^2=0.42). CO_2 evasion is least sensitive yet most tightly coupled to NPP (R^2=0.52), while CO_2 export is intermediate between the two for both (R^2=0.43) –this is expected given that CO_2 export is also the intermediate state between DOC export and CO_2 evasion. The greater scattering of DOC:NPP compared to evasion:NPP is understandable, given that the initial of leaching is a covariate of both primary production and runoff, whereas the actual evasion flux is largely dependent on organic inputs (production) and temperature.

4.8 Land-Ocean Aquatic Continuum (LOAC)

4.8.1 LOAC Fluxes

Overall, our simulation results show that dissolved carbon entering the Lena river system is significantly transformed during its transport to the ocean. Taking the average throughput of carbon into the system over the last ten years of our simulation, our results show that whereas 7 TgC yr^{-1} (after reinfiltration following flooding of 0.45 TgC yr^{-1}; see Fig. 2 'Return' flux) of carbon enters the Lena from terrestrial sources as dissolved carbon and CO_2, only 3.4 TgC yr^{-1} is discharged into the Laptev Sea and beyond from the river mouth. The remainder (3.6TgC yr^{-1}) is metabolised in the water column during transport and evaded to the atmosphere (bottom panel, Fig. 12a). The terrestrial DOC inflow estimate is comparable to that made by Kicklighter et al. (2013), who estimated in a modelling study terrestrial dissolved carbon loading of the Lena is ~7.7 TgC yr^{-1}.

The relative quantities of carbon inflow, evasion and outflow in the river system that are presented for the Lena in Fig. 12a can be compared to the same relative quantities –that is, the ratios of evasion:in and out:in, where 'in' refers to dissolved terrestrial input, – from the global study by Cole et al. (2007), who estimated these fluxes from empirical or empirically-derived data at the global scale. This is shown in the top panel of Fig. 12a, where we simplify the Cole et al. (2007) data to exclude global groundwater CO_2 flux from the coast to the ocean (because our basin mask has a single coastal pixel whereas coastal groundwater seepage is distributed along the entire continental boundary) and the POC fraction of in-river transport and sedimentation (since ORCHIDEE MICT lacks a POC erosion/sedimentation module) from their budget.

This gives global terrestrial dissolved carbon input of 1.45 PgC yr^{-1}, 0.7 PgC of which is discharged to the ocean, and the other 0.75 PgC evaded to the atmosphere. Taking the previously mentioned [evasion:in] and [out:in] ratios as a percentage, the outflow and evasion fluxes for the Lena versus the global aggregate are remarkably similar, at 48.6 vs. 48.3% and 51.4 vs 51.7%, for the two respective flows. Thus our results agree with the proposition that the riverine portion of the 'land-ocean aquatic continuum' (Regnier et al., 2013) or 'boundless carbon cycle' (Battin et al., 2009) is indeed a substantial reactor for matter transported along it.

Geosci. Model Dev. Discuss., https://doi.org/10.5194/gmd-2018-322
Manuscript under review for journal Geosci. Model Dev.
Discussion started: 25 March 2019

881 **4.8.2 LOAC drivers**
882
883 The constant climate (CLIM) and constant CO_2 (CO2) simulations were undertaken to
884 assess the extent –and the extent of the difference –to which these two factors are
885 drivers of model processes and fluxes. These differences are summarised in Figs. 12(b-
886 c), in which we show the same 1998-2007 –averaged yearly variable fluxes as in the
887 CTRL simulation, expressed as percentages of the CTRL values given in Fig. 2. A number
888 of conclusions can be drawn from these diagrams.
889
890 First, all fluxes are lower in the factorial simulations, which can be expected due to
891 lower carbon input to vegetation from the atmosphere (constant CO_2) and colder
892 temperatures (constant climate) inhibiting more vigorous growth and carbon cycling.
893 Second, broadly speaking, both climate and CO_2 appear to have similar effects on all
894 fluxes, at least within the range of climatic and CO_2 values to which they have subjected
895 the model in these historical runs. With regard to lateral export fluxes in isolation,
896 variable climate (temperature increase) is a more powerful driver than CO_2 increase
897 (see below). Third, the greatest difference between the constant climate and CO_2
898 simulation carbon fluxes appear to be those associated with terrestrial inflow of
899 dissolved matter to the aquatic network, these being more sensitive to climatic than CO_2
900 variability. This is evidenced by a 49% and 32% decline in CO_2 and DOC export,
901 respectively, from the land to rivers in the constant climate simulation, versus a 27%
902 and 23% decline in these same variables in the constant CO_2 simulation. Given that the
903 decline in primary production and respiration in both factorial simulations was roughly
904 the same, this difference in terrestrial dissolved input is attributable to the effect of
905 climate (increased temperatures) on the hydrological cycle, driving changes in lateral
906 export fluxes.
907
908 This would imply that at these carbon dioxide and climatic ranges, the modelled DOC
909 inputs are slightly more sensitive to changes in the climate rather than to changes in
910 atmospheric carbon dioxide concentration and the first order biospheric response to
911 this. However, while the model biospheric response to carbon dioxide concentration
912 may be linear, thresholds in environmental variables such as MAAT may prove to be
913 tipping points in the system's emergent response to change, as implied by Fig. 9,
914 meaning that the Lena, as with the Arctic in general, may soon become much more
915 temperature-dominated, with regard to the drivers of its own change.
916
917 **4.8.3 LOAC export flux considerations**
918
919 Despite our simulations' agreement with observations regarding the proportional fate of
920 terrestrial DOC inputs as evasion and marine export (Section 4.8.1, Fig. 12a), our results
921 suggest substantial and meaningful differences in the magnitude of those fluxes relative
922 to NPP in the Lena, compared to those estimated by other studies in temperate or
923 tropical biomes. Our simulations' cumulative DOC and CO_2 export from the terrestrial
924 realm into inland waters is equivalent to ~1.5 % of NPP.
925
926 This is considerably lower than Cole et al. (2007) and Regnier et al. (2013) who find
927 lateral transfer to approximate ~5% (1.9PgC yr^{-1}) of NPP at the global scale, while
928 Lauerwald et al. (2017) found similar rates for the Amazon. The cause of this
929 discrepancy with our results is beyond the scope of this study to definitively address,

given the lack of tracers for carbon source and age in our model. Nonetheless, our analysis leads us to hypothesise the following.

Temperature limitation of soil microbial respiration at the end of the growing season (approaching zero by October, SI Fig. S4d) makes this flux neglible from November through May (SI Fig. S4d). In late spring, mobilisation of organic carbon is performed by both microbial respiration and leaching of DOC via runoff and drainage water fluxes. However, because the latter are controlled by the initial spring meltwater flux period, which occurs before the growing season has had time to produce litter or new soil carbon (May-June, Fig. 4b), aggregate yearly DOC transport reactivity is characterised by the available plant matter from the previous year, which is overwhelmingly derived from recalcitrant soil matter (Fig. 11a) and is itself less available for leaching based on soil carbon residence times.

This causes relatively low leaching rates and riverine DOC concentration s(e.g. Fig. 9), as compared to the case of leaching from the same year's biological production. Highlighting this point are floodplains' domination by labile carbon sourced from that year's production with a mean DOC concentration of 12.4 mgC L^{-1} (1998-2007 average), with mean riverine DOC concentrations around half that value (6.9 mgC L^{-1}). Nonetheless the May-June meltwater pulse period dominates aggregate DOC discharge. As this pulse rapidly subsides by late July, so does the leaching and transport of organic matter. Warmer temperatures come in conjunction with increased primary production and the temperature driven soil heterotrophic degradation of contemporary and older matter (via active layer deepening). These all indicate that transported dissolved matter in rivers, at least at peak outflow, is dominated by sources originating in the previous year's primary production, that was literally 'frozen out' of more complete decomposition by soil heterotrophs.

Further, we infer from the fact that all of our simulation grid cells fall within areas of low (<-2°C) MAAT, far below the threshold MAAT (>3°C) proposed by Laudon et al. (2012) for soil respiration-dominated carbon cycling systems (Fig. 9), that the Lena is hydrologically-limited with respect to DOC concentration and its lateral flux. Indeed, the seasonal discharge trend of the Lena –massive snowmelt-driven hydrological and absolute DOC flux, coupled with relatively low DOC concentrations at the river mouth (Fig. 4b, simulation data of Fig. 9), are in line with the Laudon et al. (2012) typology.

We therefore suggest that relatively low lateral transport relative to primary production rates (e.g. as a percentage of net primary production, (%NPP)) in our simulations compared to the lateral transport : NPP percentages reported from the literature in other biomes is driven by meltwater (vs. precipitation) dominated DOC mobilisation, which occurs during a largely pre-litter deposition period of the growing season. DOC is then less readily mobilised by being sourced from recalcitrant matter, leading to low leaching concentrations relative to those from labile material. As discharge rates decline, the growing season reaches its peak, leaving carbon mobilisation of fresh organic matter to be overwhelmingly driven by in situ heterotrophic respiration.

While we have shown that bulk DOC fluxes scale linearly to bulk discharge flows (Fig. 3d), DOC concentrations (mgC L^{-1}) hold a more complex and weaker positive relationship with discharge rates, with correlation coefficients (R^2) of 0.05 and 0.25 for

Geosci. Model Dev. Discuss., https://doi.org/10.5194/gmd-2018-322
Manuscript under review for journal Geosci. Model Dev.
Discussion started: 25 March 2019

river and stream DOC concentrations, respectively (Fig. 13). This implies that while increasing discharge reflects increasing runoff and an increasing vector for DOC leaching, particularly in smaller tributary streams, by the time this higher input of carbon reaches the river main stem there is a confounding effect of dilution by increased water fluxes which reduces DOC concentrations, explaining the difference between stream and river discharge vs. DOC concentration regressions in the Figure. Thus, and as a broad generalisation, with increasing discharge rates we can also expect somewhat higher concentrations of terrestrial DOC input to streams and rivers. Over the floodplains, DOC concentrations hold no linear relationship with discharge rates (R^2=0.003 , SI Fig. S5), largely reflecting the fact that DOC leaching is here limited by terrestrial primary production rates more than by hydrology. To the extent that floodplains fundamentally require flooding and hence do depend on floodwater inputs at a primary level, we hypothesise that DOC leaching rates are not limited by that water input, at least over the simulated Lena basin.

As discussed above simulated DOC and CO_2 export as a percentage of simulated NPP over the Lena basin was 1.5% over 1998-2007. However, this proportion appears to be highly dynamic at the decadal timescale. As shown in Fig. 11b, all lateral flux components in our simulations increased their relative throughput at a rate double to triple that of NPP or respiration fluxes over the 20th century, also doing so at a rate substantially higher than the rate increase in discharge. In addition, differentials of these lateral flux rates with the rates of their drivers (discharge, primary production) have on average increased over the century (Fig. 11b). This suggests that there are potential additive effects of the production and discharge drivers of lateral fluxes that could lead to non-linear reponses to changes in these drivers as the Arctic environment transforms, as suggested by the Laudon et al. (2012) data plotted in Fig. 4. Acceleration of the hydrological cycle compounded by temperature and CO_2 -driven increases in primary production could therefore increase the amount of matter available for leaching, increase the carbon concentration of leachate, and increase the aggregate generation of runoff to be used as a DOC transport vector. Given that these causal dynamics apply generally to permafrost regions, both low lateral flux as %NPP and the hypothesised response of those fluxes to future warming may be a feature particular to most high latitude river basins.

5. Conclusion

This study has shown that the new DOC-representing high latitude model version of ORCHIDEE, ORCHIDEE MICT-LEAK, is able to reproduce with reasonable accuracy modern concentrations, rates and absolute fluxes of carbon in dissolved form, as well as the relative seasonality of these quantities through the year. When combined with a reasonable reproduction of real-world stream, river and floodplain dynamics, we demonstrate that this model is a potentially powerful new tool for diagnosing and reproducing past, present and potentially future states of the Arctic carbon cycle. Our simulations show that of the 34 TgC yr^{-1} remaining after GPP is respired autotrophically and heterotrophically in the Lena basin, over one-fifth of this captured carbon is removed into the aquatic system. Of this, over half is released to the atmosphere from the river surface during its period of transport to the ocean, in agreement with previous empirically-derived global-scale studies. Both this transport and its transformation are therefore non-trivial components of the carbon system at these latitudes that we have

shown are sensitive to changes in temperature, precipitation and atmospheric CO_2 concentration. Our results, in combination with empirical data, further suggest that changes to these drivers –in particular climate –may provoke non-linear responses in the transport and transformation of carbon across the terrestrial-aquatic system's interface as change progresses in an Arctic environment increasingly characterised by amplified warming.

Code and data availability

The source code for ORCHIDEE MICT-LEAK revision 5459 is available via http://forge.ipsl.jussieu.fr/orchidee/wiki/GroupActivities/CodeAvalaibilityPublication/ORCHIDEE_gmd-2018-MICT-LEAK_r5459

Primary data and scripts used in the analysis and other supplementary information that may be useful in reproducing the author's work can be obtained by contacting the corresponding author.

This software is governed by the CeCILL license under French law and abiding by the rules of distribution of free software. You can use, modify and/or redistribute the software under the terms of the CeCILL license as circulated by CEA, CNRS and INRIA at the following URL: http://www.cecill.info.

Authors' contribution

SB coded this model version, conducted the simulations and wrote the main body of the paper. RL gave consistent input to the coding process and made numerous code improvements and bug fixes. BG advised on the inclusion of priming processes in the model and advised on the study design and model configuration; DZ gave input on the modelled soil carbon processes and model configuration. PR contributed to the interpretation of results and made substantial contributions to the manuscript text. MG, AT and AD contributed to improvements in hydrological representation and floodplain forcing data. PC oversaw all developments leading to the publication of this study. All authors contributed to suggestions regarding the final content of the study.

Competing interests

The authors declare no competing financial interests.

Acknowledgements

Simon Bowring acknowledges funding from the European Union's Horizon 2020 research and innovation program under the Marie Sklodowska-Curie grant agreement No. 643052, 'C-CASCADES' program. Simon Bowring received a PhD grant. Matthieu Guimberteau acknowledges funding from the European Research Council Synergy grant ERC-2013-SyG-610028 IMBALANCE-P. RL acknowledges funding from the European Union's Horizon 2020 research and innovation program under grant agreement no.703813 for the Marie Sklodowska-Curie European Individual Fellowship "C-Leak".

References:

Battin, T. J., Luyssaert, S., Kaplan, L. A., Aufdenkampe, A. K., Richter, A. and Tranvik, L. J.:

1077 The boundless carbon cycle, Nat. Geosci., doi:10.1038/ngeo618, 2009.
1078 Beer, C., Lucht, W., Schmullius, C. and Shvidenko, A.: Small net carbon dioxide uptake by
1079 Russian forests during 1981-1999, Geophys. Res. Lett., doi:10.1029/2006GL026919,
1080 2006.
1081 Bekryaev, R. V., Polyakov, I. V. and Alexeev, V. A.: Role of polar amplification in long-term
1082 surface air temperature variations and modern arctic warming, J. Clim.,
1083 doi:10.1175/2010JCLI3297.1, 2010.
1084 Cauwet, G. and Sidorov, I.: The biogeochemistry of Lena River: Organic carbon and
1085 nutrients distribution, in Marine Chemistry., 1996.
1086 Cole, J. J., Prairie, Y. T., Caraco, N. F., McDowell, W. H., Tranvik, L. J., Striegl, R. G., Duarte,
1087 C. M., Kortelainen, P., Downing, J. A., Middelburg, J. J. and Melack, J.: Plumbing the global
1088 carbon cycle: Integrating inland waters into the terrestrial carbon budget, Ecosystems,
1089 doi:10.1007/s10021-006-9013-8, 2007.
1090 Connolly, C. T., Khosh, M. S., Burkart, G. A., Douglas, T. A., Holmes, R. M., Jacobson, A. D.,
1091 Tank, S. E. and McClelland, J. W.: Watershed slope as a predictor of fluvial dissolved
1092 organic matter and nitrate concentrations across geographical space and catchment size
1093 in the Arctic, Environ. Res. Lett., 13(10), 104015, doi:10.1088/1748-9326/aae35d, 2018.
1094 DeLuca, T. H. and Boisvenue, C.: Boreal forest soil carbon: Distribution, function and
1095 modelling, Forestry, doi:10.1093/forestry/cps003, 2012.
1096 Denfeld, B., Frey, K. and Sobczak, W.: Summer CO 2 evasion from streams and rivers in
1097 the Kolyma River basin, north-east Siberia, Polar …, doi:10.3402/polar.v32i0.19704,
1098 2013.
1099 Dolman, A. J., Shvidenko, A., Schepaschenko, D., Ciais, P., Tchebakova, N., Chen, T., Van
1100 Der Molen, M. K., Belelli Marchesini, L., Maximov, T. C., Maksyutov, S. and Schulze, E. D.:
1101 An estimate of the terrestrial carbon budget of Russia using inventory-based, eddy
1102 covariance and inversion methods, Biogeosciences, doi:10.5194/bg-9-5323-2012, 2012.
1103 Drake, T. W., Wickland, K. P., Spencer, R. G. M., McKnight, D. M. and Striegl, R. G.: Ancient
1104 low–molecular-weight organic acids in permafrost fuel rapid carbon dioxide production
1105 upon thaw, Proc. Natl. Acad. Sci., doi:10.1073/pnas.1511705112, 2015.
1106 Elberling, B.: Annual soil CO2effluxes in the High Arctic: The role of snow thickness and
1107 vegetation type, Soil Biol. Biochem., doi:10.1016/j.soilbio.2006.09.017, 2007.
1108 Frey, K. E. and McClelland, J. W.: Impacts of permafrost degradation on arctic river
1109 biogeochemistry, Hydrol. Process., doi:10.1002/hyp.7196, 2009.
1110 Frey, K. E. and Smith, L. C.: Amplified carbon release from vast West Siberian peatlands
1111 by 2100, Geophys. Res. Lett., doi:10.1029/2004GL022025, 2005.
1112 Guimberteau, M., Zhu, D., Maignan, F., Huang, Y., Yue, C., Dantec-N d lec, S., Ottl, C., Jornet-
1113 Puig, A., Bastos, A., Laurent, P., Goll, D., Bowring, S., Chang, J., Guenet, B., Tifafi, M., Peng,
1114 S., Krinner, G., Ducharne, A. s., Wang, F., Wang, T., Wang, X., Wang, Y., Yin, Z., Lauerwald,
1115 R., Joetzjer, E., Qiu, C., Kim, H. and Ciais, P.: ORCHIDEE-MICT (v8.4.1), a land surface
1116 model for the high latitudes: model description and validation, Geosci. Model Dev.,
1117 doi:10.5194/gmd-11-121-2018, 2018.
1118 Holmes, R. M., McClelland, J. W., Peterson, B. J., Tank, S. E., Bulygina, E., Eglinton, T. I.,
1119 Gordeev, V. V., Gurtovaya, T. Y., Raymond, P. A., Repeta, D. J., Staples, R., Striegl, R. G.,
1120 Zhulidov, A. V. and Zimov, S. A.: Seasonal and Annual Fluxes of Nutrients and Organic
1121 Matter from Large Rivers to the Arctic Ocean and Surrounding Seas, Estuaries and
1122 Coasts, doi:10.1007/s12237-011-9386-6, 2012.
1123 Jasechko, S., Kirchner, J. W., Welker, J. M. and McDonnell, J. J.: Substantial proportion of
1124 global streamflow less than three months old, Nat. Geosci., doi:10.1038/ngeo2636, 2016.
1125 Kaiser, K. and Kalbitz, K.: Cycling downwards - dissolved organic matter in soils, Soil

Biol. Biochem., doi:10.1016/j.soilbio.2012.04.002, 2012.
Kicklighter, D. W., Hayes, D. J., Mcclelland, J. W., Peterson, B. J., Mcguire, A. D. and Melillo, J. M.: Insights and issues with simulating terrestrial DOC loading of Arctic river networks, Ecol. Appl., doi:10.1890/11-1050.1, 2013.
Klaminder, J., Grip, H., Mörth, C. M. and Laudon, H.: Carbon mineralization and pyrite oxidation in groundwater: Importance for silicate weathering in boreal forest soils and stream base-flow chemistry, Appl. Geochemistry, doi:10.1016/j.apgeochem.2010.12.005, 2011.
Kutscher, L., Mörth, C. M., Porcelli, D., Hirst, C., Maximov, T. C., Petrov, R. E. and Andersson, P. S.: Spatial variation in concentration and sources of organic carbon in the Lena River, Siberia, J. Geophys. Res. Biogeosciences, doi:10.1002/2017JG003858, 2017.
Lammers, R. B., Shiklomanov, A. I., Vörösmarty, C. J., Fekete, B. M. and Peterson, B. J.: Assessment of contemporary Arctic river runoff based on observational discharge records, J. Geophys. Res. Atmos., doi:10.1029/2000JD900444, 2001.
Lara, R. J., Rachold, V., Kattner, G., Hubberten, H. W., Guggenberger, G., Skoog, A. and Thomas, D. N.: Dissolved organic matter and nutrients in the Lena River, Siberian Arctic: Characteristics and distribution, Mar. Chem., doi:10.1016/S0304-4203(97)00076-5, 1998.
Laudon, H., Buttle, J., Carey, S. K., McDonnell, J., McGuire, K., Seibert, J., Shanley, J., Soulsby, C. and Tetzlaff, D.: Cross-regional prediction of long-term trajectory of stream water DOC response to climate change, Geophys. Res. Lett., doi:10.1029/2012GL053033, 2012.
Lauerwald, R., Hartmann, J., Ludwig, W. and Moosdorf, N.: Assessing the nonconservative fluvial fluxes of dissolved organic carbon in North America, J. Geophys. Res. Biogeosciences, doi:10.1029/2011JG001820, 2012.
Lauerwald, R., Regnier, P., Camino-Serrano, M., Guenet, B., Guimberteau, M., Ducharne, A., Polcher, J. and Ciais, P.: ORCHILEAK (revision 3875): A new model branch to simulate carbon transfers along the terrestrial-aquatic continuum of the Amazon basin, Geosci. Model Dev., doi:10.5194/gmd-10-3821-2017, 2017.
Lloyd, J., Shibistova, O., Zolotoukhine, D., Kolle, O., Arneth, A., Wirth, C., Styles, J. M., Tchebakova, N. M. and Schulze, E. D.: Seasonal and annual variations in the photosynthetic productivity and carbon balance of a central Siberian pine forest, Tellus, Ser. B Chem. Phys. Meteorol., doi:10.1034/j.1600-0889.2002.01487.x, 2002.
Mann, P. J., Eglinton, T. I., McIntyre, C. P., Zimov, N., Davydova, A., Vonk, J. E., Holmes, R. M. and Spencer, R. G. M.: Utilization of ancient permafrost carbon in headwaters of Arctic fluvial networks, Nat. Commun., doi:10.1038/ncomms8856, 2015.
McGuire, K. J., McDonnell, J. J., Weiler, M., Kendall, C., McGlynn, B. L., Welker, J. M. and Seibert, J.: The role of topography on catchment-scale water residence time, Water Resour. Res., doi:10.1029/2004WR003657, 2005.
Nachtergaele, F. et al.: The harmonized world soil database, FAO, ISRIC,ISSCAS, JRC, doi:3123, 2010.
Qiu, C., Zhu, D., Ciais, P., Guenet, B., Krinner, G., Peng, S., Aurela, M., Bernhofer, C., Brümmer, C., Bret-Harte, S., Chu, H., Chen, J., Desai, A. R., Dušek, J., Euskirchen, E. S., Fortuniak, K., Flanagan, L. B., Friborg, T., Grygoruk, M., Gogo, S., Grünwald, T., Hansen, B. U., Holl, D., Humphreys, E., Hurkuck, M., Kiely, G., Klatt, J., Kutzbach, L., Largeron, C., Laggoun-Défarge, F., Lund, M., Lafleur, P. M., Li, X., Mammarella, I., Merbold, L., Nilsson, M. B., Olejnik, J., Ottosson-Löfvenius, M., Oechel, W., Parmentier, F. J. W., Peichl, M., Pirk, N., Peltola, O., Pawlak, W., Rasse, D., Rinne, J., Shaver, G., Peter Schmid, H., Sottocornola, M., Steinbrecher, R., Sachs, T., Urbaniak, M., Zona, D. and Ziemblinska, K.: ORCHIDEE-

PEAT (revision 4596), a model for northern peatland CO2, water, and energy fluxes on daily to annual scales, Geosci. Model Dev., doi:10.5194/gmd-11-497-2018, 2018.

Raymond, P. A., McClelland, J. W., Holmes, R. M., Zhulidov, A. V., Mull, K., Peterson, B. J., Striegl, R. G., Aiken, G. R. and Gurtovaya, T. Y.: Flux and age of dissolved organic carbon exported to the Arctic Ocean: A carbon isotopic study of the five largest arctic rivers, Global Biogeochem. Cycles, doi:10.1029/2007GB002934, 2007.

Regnier, P., Friedlingstein, P., Ciais, P., Mackenzie, F. T., Gruber, N., Janssens, I. A., Laruelle, G. G., Lauerwald, R., Luyssaert, S., Andersson, A. J., Arndt, S., Arnosti, C., Borges, A. V., Dale, A. W., Gallego-Sala, A., Goddéris, Y., Goossens, N., Hartmann, J., Heinze, C., Ilyina, T., Joos, F., Larowe, D. E., Leifeld, J., Meysman, F. J. R., Munhoven, G., Raymond, P. A., Spahni, R., Suntharalingam, P. and Thullner, M.: Anthropogenic perturbation of the carbon fluxes from land to ocean, Nat. Geosci., doi:10.1038/ngeo1830, 2013.

Roser, C., Montagnani, L., Schulze, E.-D., Mollicone, D., Kolle, O., Meroni, M., Papale, D., Marchesini, L. B., Federici, S. and Valentini, R.: Net CO2 exchange rates in three different successional stages of the "Dark Taiga" of central Siberia, Tellus B, doi:10.1034/j.1600-0889.2002.01351.x, 2002.

Sawamoto, T., Hatano, R., Yajima, T., Takahashi, K. and Isaev, A. P.: Soil respiration in siberian taiga ecosystems with different histories of forest fire, Soil Sci. Plant Nutr., doi:10.1080/00380768.2000.10408759, 2000.

Schulze, E. D., Lloyd, J., Kelliher, F. M., Wirth, C., Rebmann, C., Luhker, B., Mund, M., Knohl, A., Milyukova, I. M., Schulze, W., Ziegler, W., Varlagin, A. B., Sogachev, A. F., Valentini, R., Dore, S., Grigoriev, S., Kolle, O., Panfyorov, M. I., Tchebakova, N. and Vygodskaya, N. N.: Productivity of forests in the eurosiberian boreal region and their potential to act as a carbon sink - a synthesis, Glob. Chang. Biol., doi:10.1046/j.1365-2486.1999.00266.x, 1999.

Semiletov, I. P., Pipko, I. I., Shakhova, N. E., Dudarev, O. V., Pugach, S. P., Charkin, A. N., Mcroy, C. P., Kosmach, D. and Gustafsson, Ö.: Carbon transport by the Lena River from its headwaters to the Arctic Ocean, with emphasis on fluvial input of terrestrial particulate organic carbon vs. carbon transport by coastal erosion, Biogeosciences, doi:10.5194/bg-8-2407-2011, 2011.

Shvartsev, S. L.: Geochemistry of fresh groundwater in the main landscape zones of the Earth, Geochemistry Int., doi:10.1134/S0016702908130016, 2008.

Shvidenko, A. and Nilsson, S.: A synthesis of the impact of Russian forests on the global carbon budget for 1961-1998, Tellus, Ser. B Chem. Phys. Meteorol., doi:10.1034/j.1600-0889.2003.00046.x, 2003.

Sommerkorn, M.: Micro-topographic patterns unravel controls of soil water and temperature on soil respiration in three Siberian tundra systems, Soil Biol. Biochem., doi:10.1016/j.soilbio.2008.03.002, 2008.

Tarnocai, C., Canadell, J. G., Schuur, E. A. G., Kuhry, P., Mazhitova, G. and Zimov, S.: Soil organic carbon pools in the northern circumpolar permafrost retion, Global Biogeochem. Cycles, doi:Gb2023\n10.1029/2008gb003327, 2009.

Tootchi, A., Jost, A. and Ducharne, A.: Multi-source global wetland maps combining surface water imagery and groundwater constraints, Earth Syst. Sci. Data, doi:10.5194/essd-11-189-2019, 2019.

Vonk, J. E., Mann, P. J., Davydov, S., Davydova, A., Spencer, R. G. M., Schade, J., Sobczak, W. V., Zimov, N., Zimov, S., Bulygina, E., Eglinton, T. I. and Holmes, R. M.: High biolability of ancient permafrost carbon upon thaw, Geophys. Res. Lett., doi:10.1002/grl.50348, 2013.

Vonk, J. E., Tank, S. E., Mann, P. J., Spencer, R. G. M., Treat, C. C., Striegl, R. G., Abbott, B. W. and Wickland, K. P.: Biodegradability of dissolved organic carbon in permafrost soils and

aquatic systems: A meta-analysis, Biogeosciences, doi:10.5194/bg-12-6915-2015, 2015a.
Vonk, J. E., Tank, S. E., Bowden, W. B., Laurion, I., Vincent, W. F., Alekseychik, P., Amyot, M., Billet, M. F., Canário, J., Cory, R. M., Deshpande, B. N., Helbig, M., Jammet, M., Karlsson, J., Larouche, J., MacMillan, G., Rautio, M., Walter Anthony, K. M. and Wickland, K. P.: Reviews and Syntheses: Effects of permafrost thaw on arctic aquatic ecosystems, Biogeosciences Discuss., doi:10.5194/bgd-12-10719-2015, 2015b.
Ye, B., Yang, D., Zhang, Z. and Kane, D. L.: Variation of hydrological regime with permafrost coverage over Lena Basin in Siberia, J. Geophys. Res. Atmos., doi:10.1029/2008JD010537, 2009.
Zhang, X., Hutchings, J. A., Bianchi, T. S., Liu, Y., Arellano, A. R. and Schuur, E. A. G.: Importance of lateral flux and its percolation depth on organic carbon export in Arctic tundra soil: Implications from a soil leaching experiment, J. Geophys. Res. Biogeosciences, doi:10.1002/2016JG003754, 2017.

Tables and Figures:

Table 1: Summary describing of the factorial simulations undertaken to examine the relative drivers of lateral fluxes in our model.

Simulation Name	Abbreviation	Historical Input Data	Input* Held Constant
Control	CTRL	Climate, CO2, Vegetation	None
Constant Climate	CLIM	CO2, Vegetation	Climate
Constant CO2	CO2	Climate, Vegetation	CO2 (Pre-industrial)

*Historically-variable input

Table 2: Mean observed groundwater CO_2 and DOC concentrations for global permafrost regions subdivided by biogeographic province and compiled by Shvartsev (2008) from over 9000 observations.

	Permafrost Groundwater Provinces				
	Swamp	Tundra	Taiga	Average	Average (-Swamp)
CO_2 (mgC L^{-1})	12.3	14	10.8	12.4	12.4
DOC (mgC L^{-1})	17.6	10.1	9.3	12.3	9.7

Table 3: Summary of the average carbon reactivity types comprising the hydrological inputs to rivers and streams (runoff, drainage and floodplain inputs), and within the rivers and streams themselves, subdivided between the 'North' and 'South' of the Lena basin (greater or less than 63N, respectively).

Hydrological Source	Model Carbon Reactivity Pool	North	South
Runoff Input	Refractory	81%	83%
	Labile	19%	17%

Geosci. Model Dev. Discuss., https://doi.org/10.5194/gmd-2018-322
Manuscript under review for journal Geosci. Model Dev.
Discussion started: 25 March 2019

Drainage Input	Refractory	96%	94%
	Labile	4%	6%
Flood Input	Refractory	36%	37%
	Labile	64%	63%
Streams	Refractory	91%	89%
	Labile	9%	11%
Rivers	Refractory	92%	90%
	Labile	8%	10%

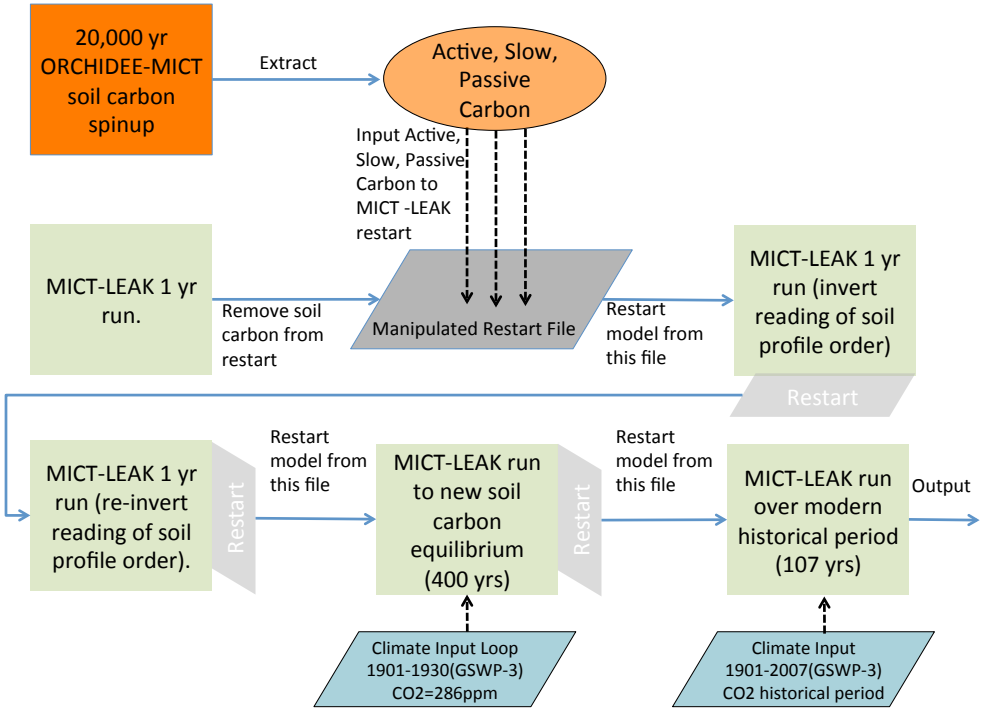

Figure 1: Flow diagram illustrating the step-wise stages required to set up the model, up to and including the historical period. The two stages that refer to the inverted reading of restart soil profile order point to the fact that the restart inputs from ORCHIDEE-MICT are read by our model in inverse order, so that one year must be run in which an activated flag reads it properly, before the reading of soil profile restarts is re-inverted for all subsequent years.

Geosci. Model Dev. Discuss., https://doi.org/10.5194/gmd-2018-322
Manuscript under review for journal Geosci. Model Dev.
Discussion started: 25 March 2019

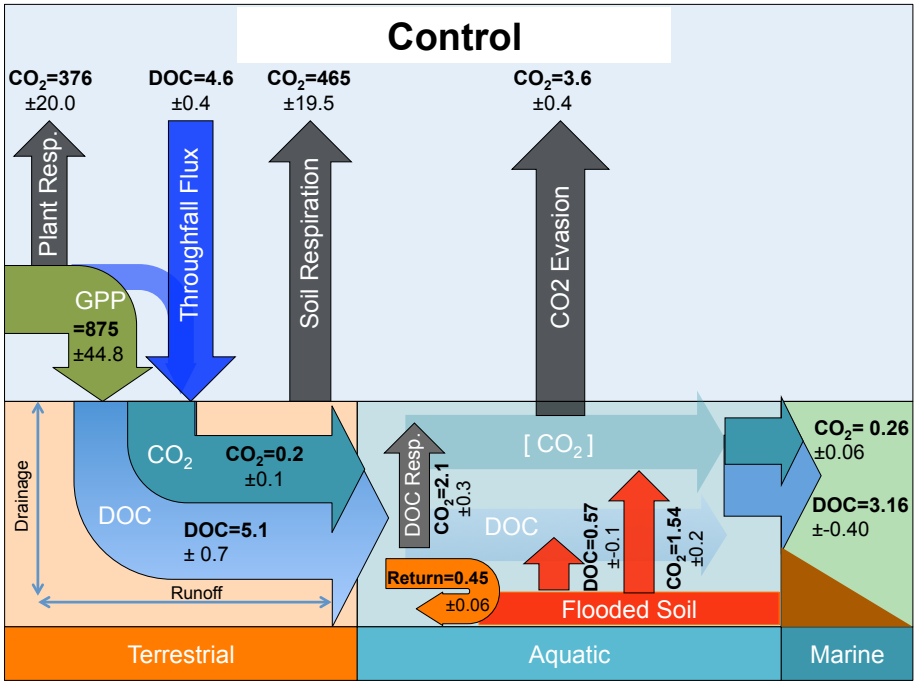

Figure 2: Schematic diagrams detailing the major yearly carbon flux outputs (TgC yr^{-1}) from the Control simulation averaged over the period 1998-2007 as they are transformed and transported across the land-aquatic continuum.

Geosci. Model Dev. Discuss., https://doi.org/10.5194/gmd-2018-322
Manuscript under review for journal Geosci. Model Dev.
Discussion started: 25 March 2019

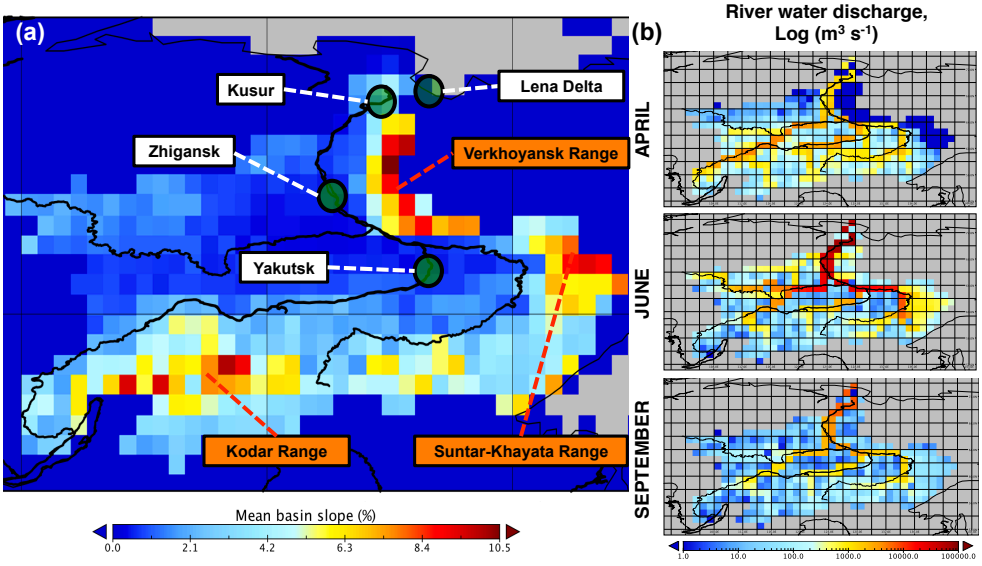

1275
1276
1277

Geosci. Model Dev. Discuss., https://doi.org/10.5194/gmd-2018-322
Manuscript under review for journal Geosci. Model Dev.
Discussion started: 25 March 2019

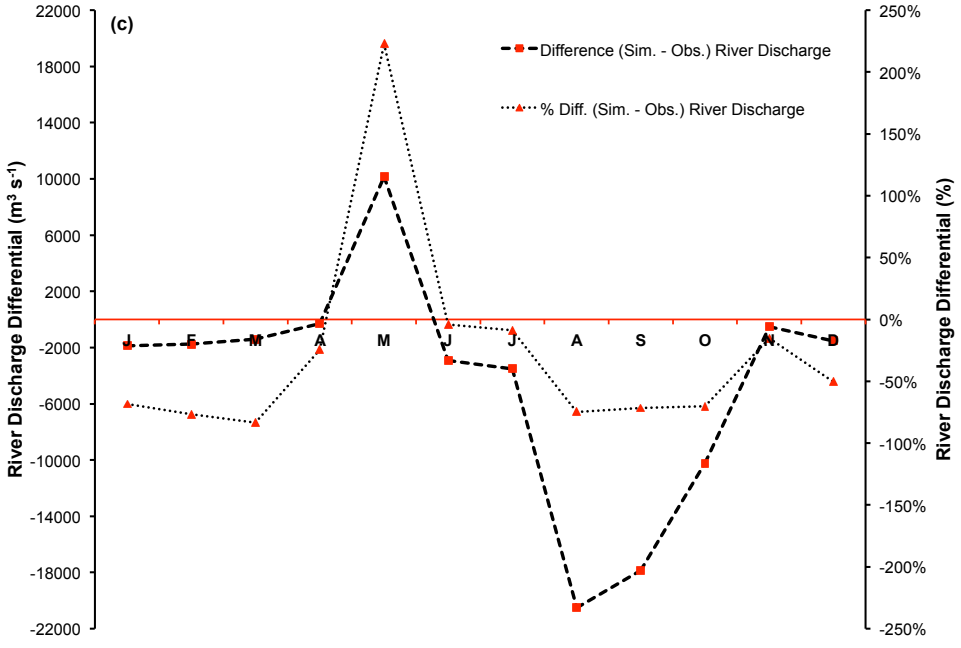

1278
1279

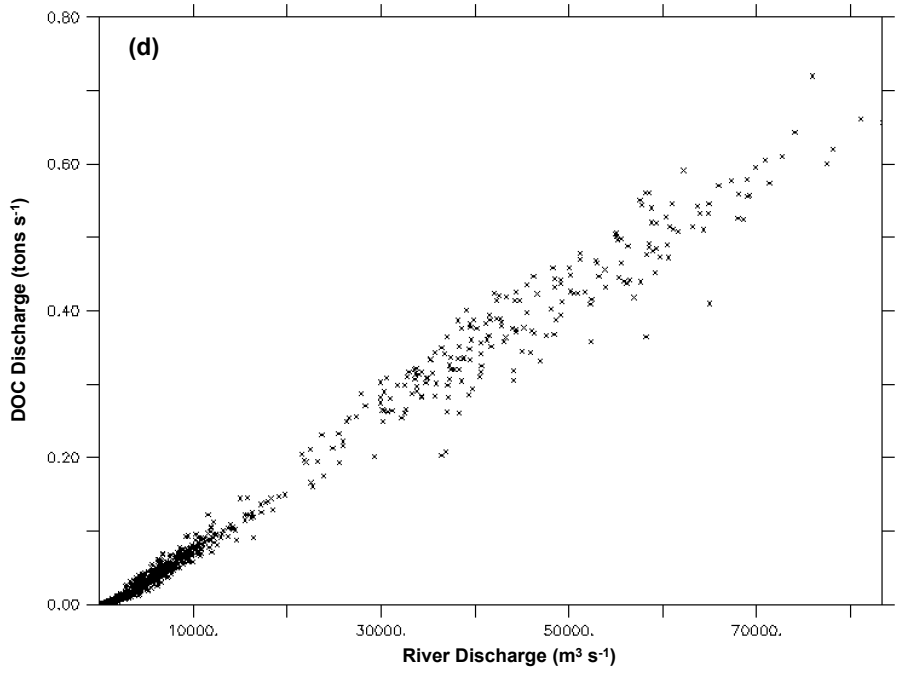

1280

Geosci. Model Dev. Discuss., https://doi.org/10.5194/gmd-2018-322
Manuscript under review for journal Geosci. Model Dev.
Discussion started: 25 March 2019

Figure 3: Map of the Lena **(a)** with the scale bar showing the mean grid cell topographic slope from the simulation, and the black line the satellite-derived overlay of the river main stem and sub-basins. Mountain ranges of the Lena basin are shown in orange. Green circles denote the outflow gridcell (Kusur) from which our simulation outflow data are derived, as well as the Zhigansk site, from which out evaluation against data from Raymond et al. (2007) are assessed. The regional capital (Yakutsk) is also included for geographic reference. **(b)** Maps of river water discharge (log(m^3 s^{-1})) in April, June and September, averaged over 1998-2007. **(c)** The mean monthly river discharge differential between observed discharge for the Lena (Ye et al., 2009) and simulated discharge averaged over 1998-2007, in absolute (m^3 s^{-1}) and percentage terms. **(d)** Regression of simulated monthly DOC discharge versus simulated river discharge at the river mouth (Kusur) over the entire simulation period (1901-2007).

(a)

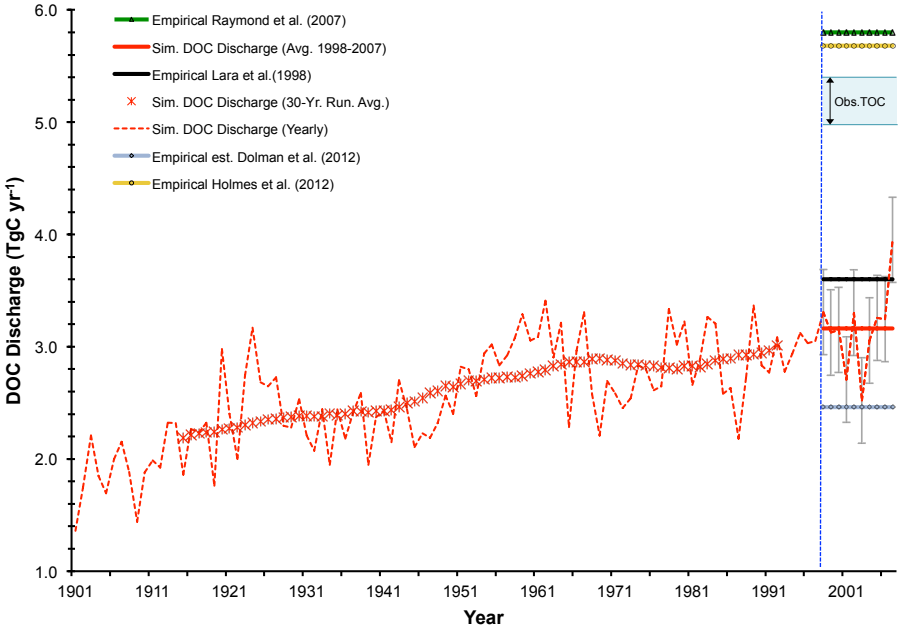

(b)

Geosci. Model Dev. Discuss., https://doi.org/10.5194/gmd-2018-322
Manuscript under review for journal Geosci. Model Dev.
Discussion started: 25 March 2019

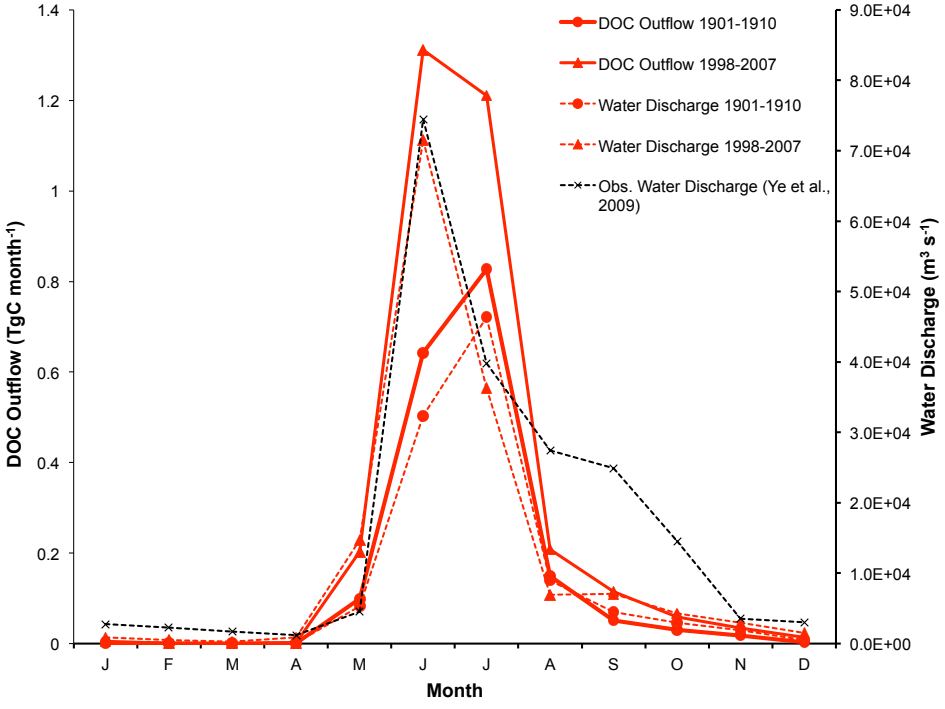

1298
1299 **(c)**

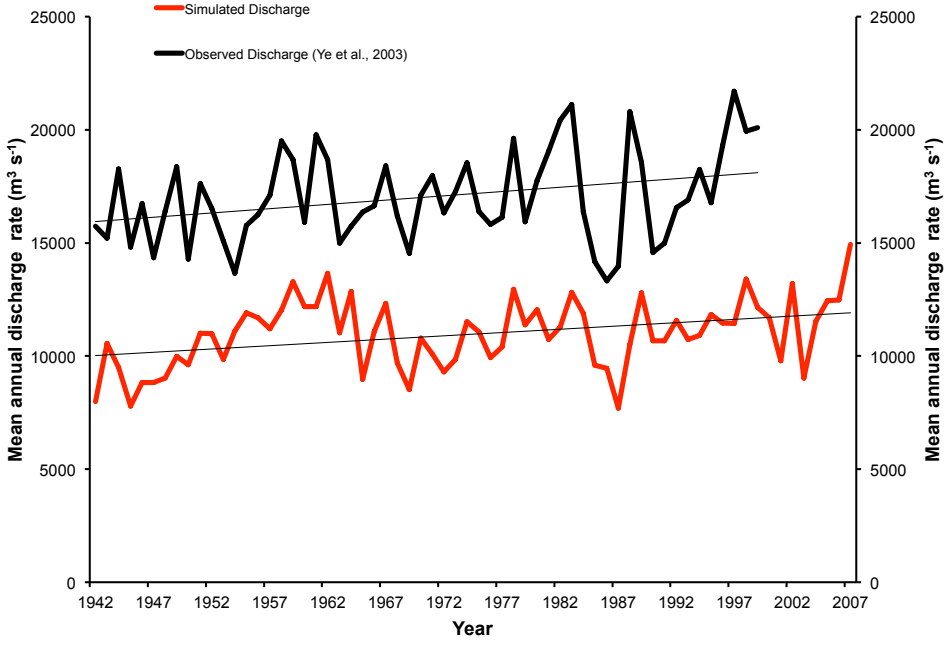

1300

Geosci. Model Dev. Discuss., https://doi.org/10.5194/gmd-2018-322
Manuscript under review for journal Geosci. Model Dev.
Discussion started: 25 March 2019

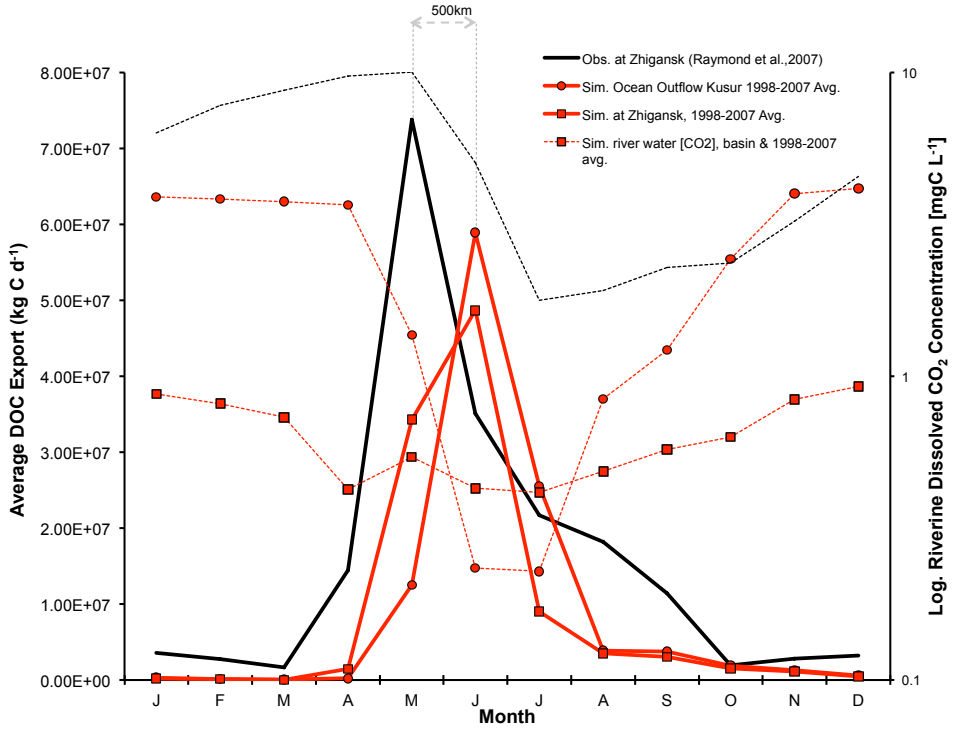

Figure 4: **(a)** Yearly DOC discharged from the Lena river into the Laptev sea is shown here in tC yr^{-1}, over the entire simulation period (dashed red line), with the smoothed, 30-year running mean shown in asterisk. Observation based estimates for DOC discharge from Lara et al. (1998), Raymond et al. (2007), Dolman et al. (2012) and Holmes et al. (2012) are shown by the horizontal black, green triangle, blue diamond and yellow circle line colours and symbols, respectively, and are to be compared against the simulated mean over the last decade of simulation (1998-2007, horizontal red line), with error bars added in grey displaying the standard deviation of simulated values over that period. The range of estimates for total organic carbon discharged as shown in Lara et al. (1998) are shown by the blue bounded region, where TOC here refers to DOC+POC. **(b)** Average monthly DOC discharge (solid red, tC $month^{-1}$) and water discharge (dashed red, m^3 s^{-1}) to the Laptev Sea over the period averaged for 1901-1910 (circles) and 1997-2007 (squares) are compared, with modern maxima closely tracking observed values. Observed water discharge over 1936-2000 from R-ArcticNet v.4 (Lammers et al., 2001) and published in Ye et al. (2009) are shown by the dashed black line. (c) **(d)** Observed (black) and simulated (red) seasonal DOC fluxes (solid lines) and CO_2 discharge concentrations (dashed lines). Observed DOC discharge as published in Raymond et al. (2007) from 2004-2005 observations at Zhigansk, a site ~500km upstream of the Lena delta. This is plotted against simulated discharge for: (i) the Lena delta at Kusur (red circles) and (ii) the approximate grid pixel corresponding to the Zhigansk site (red squares) averaged over 1998-2008. Observed CO_2 discharge from a downstream site (Cauwet & Sidorov, 1996; dashed black), and simulated from the

Geosci. Model Dev. Discuss., https://doi.org/10.5194/gmd-2018-322
Manuscript under review for journal Geosci. Model Dev.
Discussion started: 25 March 2019

outflow site (dashed circle) and the basin average (dashed square) are shown on the log-scale right-hand axis for 1998-2008.

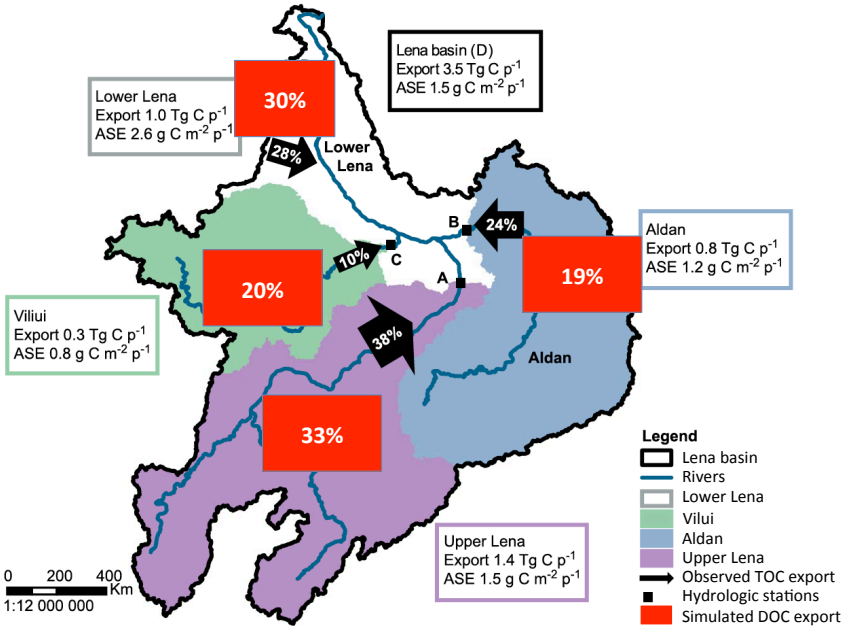

Figure 5: Map adapted from Fig. 2 in Kutscher et al. (2017) showing proportional sub-basin contributions of TOC outflow to total TOC discharge in 2012-2013 as observed in Kutscher et al., 2017 (black arrows), and DOC export contributions as simulated over the period 1998-2007 by ORCHIDEE MICT-L (red boxes). Simulation pixels used in the calculation are correlates of the real-world sampling locations unless the site coordinates deviated from a mainstem hydrographic flowpath pixel –in which case a nearest 'next-best' pixel was used. Here the percentages are out of the summed mean bulk DOC flow of each tributary, not the mean DOC discharge from the river mouth, because doing so would negate the in-stream loss of DOC via degradation to CO_2 while in-stream.

Geosci. Model Dev. Discuss., https://doi.org/10.5194/gmd-2018-322
Manuscript under review for journal Geosci. Model Dev.
Discussion started: 25 March 2019

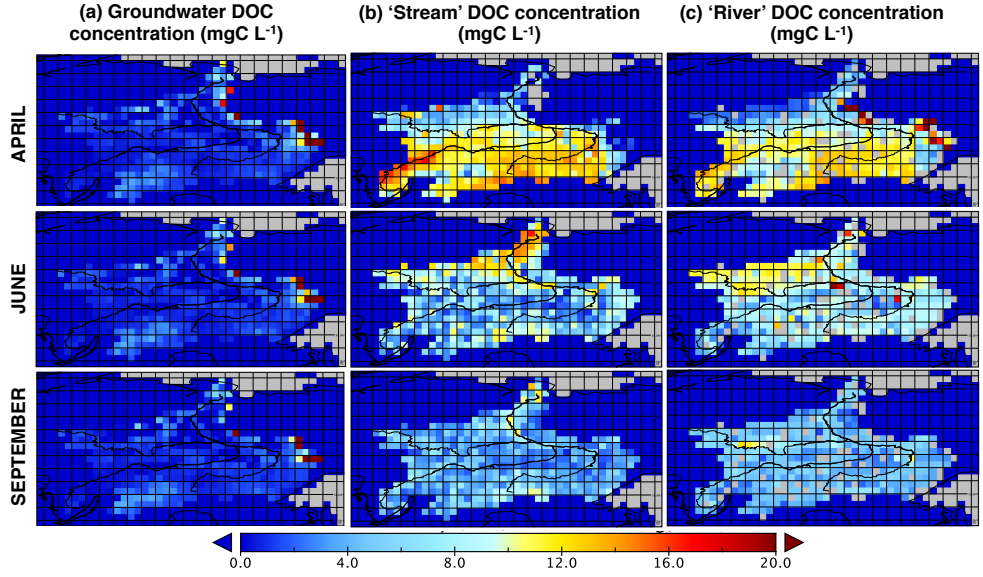

Figure 6: Maps of **(a)** DOC concentrations (mgC L^{-1}) in groundwater ('slow' water pool), **(b)** stream water pool, **(c)** river water pool in April, June and September (first to third rows, respectively), averaged over the period 1998-2007. The coastal boundary and a water body overlay have been applied to the graphic in black, and the same scale applies to all diagrams.

(a)

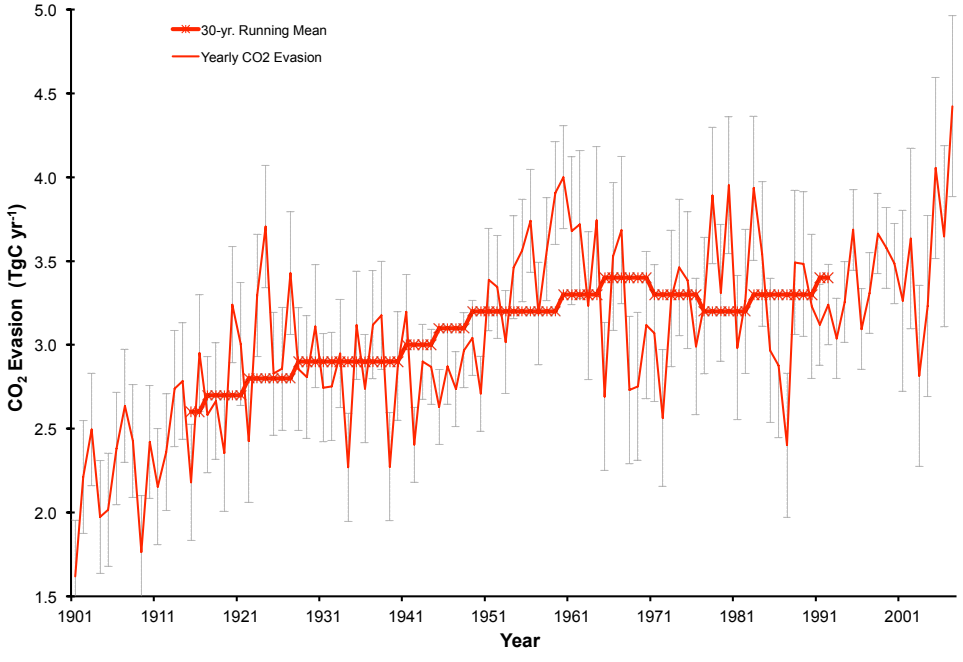

Geosci. Model Dev. Discuss., https://doi.org/10.5194/gmd-2018-322
Manuscript under review for journal Geosci. Model Dev.
Discussion started: 25 March 2019

1352 **(b)**

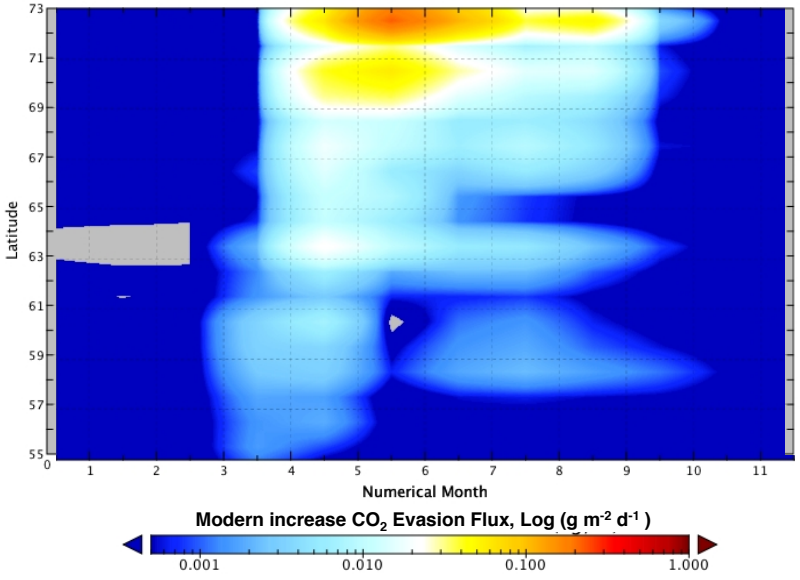

1353
1354 **(c)**

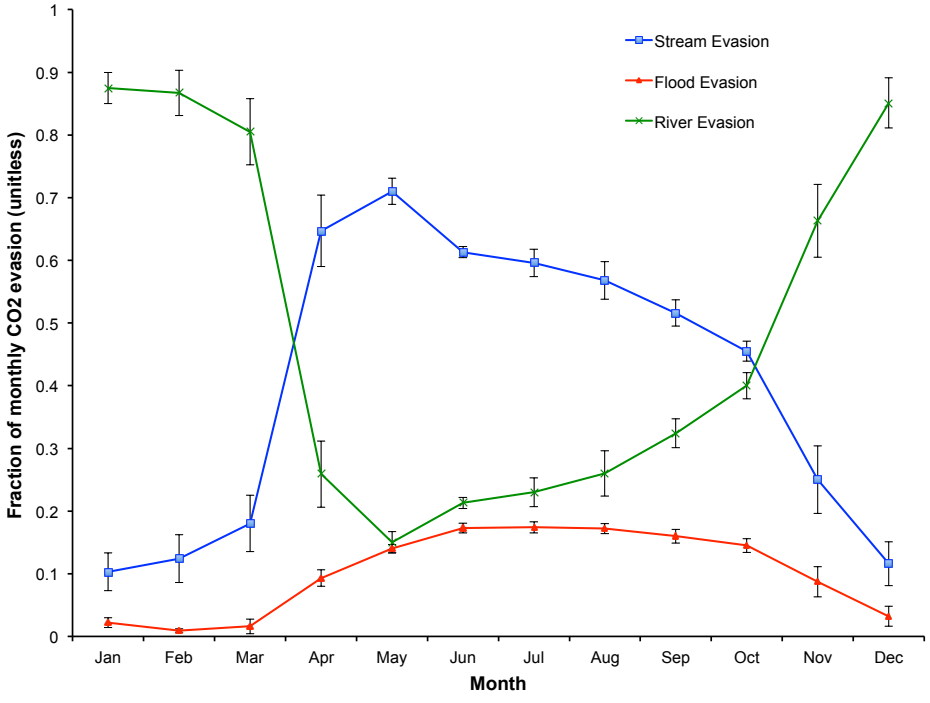

1355
1356 **(d)**

Geosci. Model Dev. Discuss., https://doi.org/10.5194/gmd-2018-322
Manuscript under review for journal Geosci. Model Dev.
Discussion started: 25 March 2019

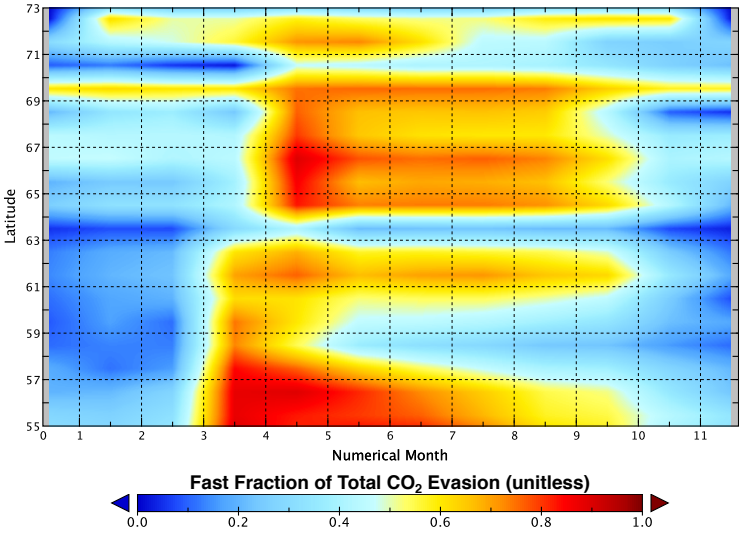

(e)

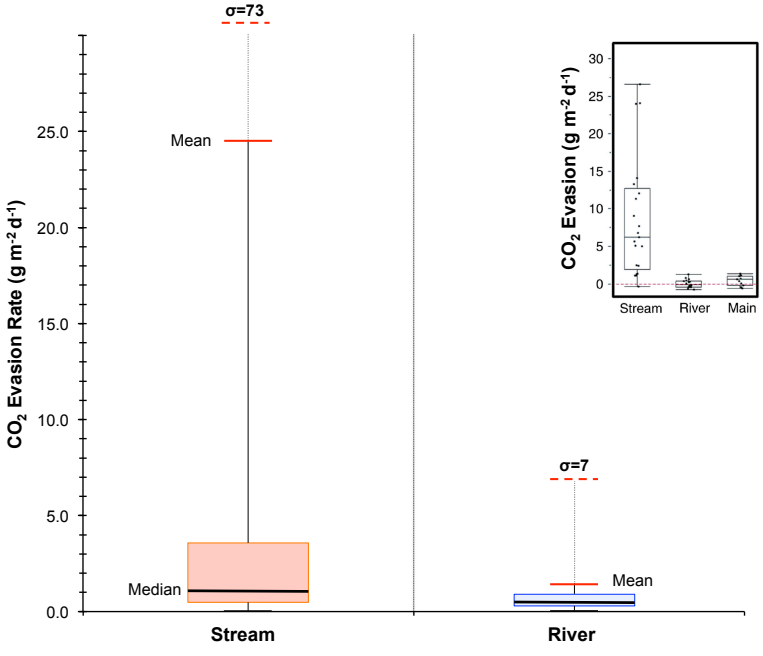

Figure 7: CO_2 evasion from stream, river, flood reservoirs. **(a)** Timeseries of total yearly CO_2 evasion (tC yr^{-1}) summed over the three hydrological pools (red line) with

Geosci. Model Dev. Discuss., https://doi.org/10.5194/gmd-2018-322
Manuscript under review for journal Geosci. Model Dev.
Discussion started: 25 March 2019

Geoscientific Model Development Discussions

the 30-year running mean of the same variable overlain in thick red (askterisk). Error bars give the standard deviation of each decade (e.g. 1901-1910) for each data point in that decade. **(b)** Log-scale Hovmöller diagram plotting the longitudinally-averaged difference (increase) in total CO_2 evaded from the Lena River basin between the average of the periods 1998-2007 and 1901-1910, over each montly timestep, in (log) gC m^{-2} d^{-1}. Thus as the river drains northward the month-on-month difference in water-body CO_2 flux, between the beginning and end of the 20th Century is shown; **(c)** The fraction of total CO_2 evasion emitted from each of the hydrological pools for the average of each month over the period 1998-2007 is shown for river, flood and stream pools (blue, green and red lines, respectively), with error bars depicting the standard deviation of data values for each month displayed. **(d)** Hovmöller diagram showing the monthly evolution of the stream pool fraction (range 0-1) per month and per latitudinal band, averaged over the period 1998-2007. **(e)** Boxplot for approximate (see text) simulated CO_2 evasion (gC m^{-2} d^{-1}) from the streamwater reservoir and river water reservoir averaged over 1998-2007. Coloured boxes denote the first and third quartiles of the data range, internal black bars the median. Whiskers give the mean (solid red bar) and standard deviation (dashed red bar) of the respective data. Empirical data on these quantities using the same scale for rivers, streams and mainstem of the Kolyma river from Denfeld et al., 2013 are shown inset.

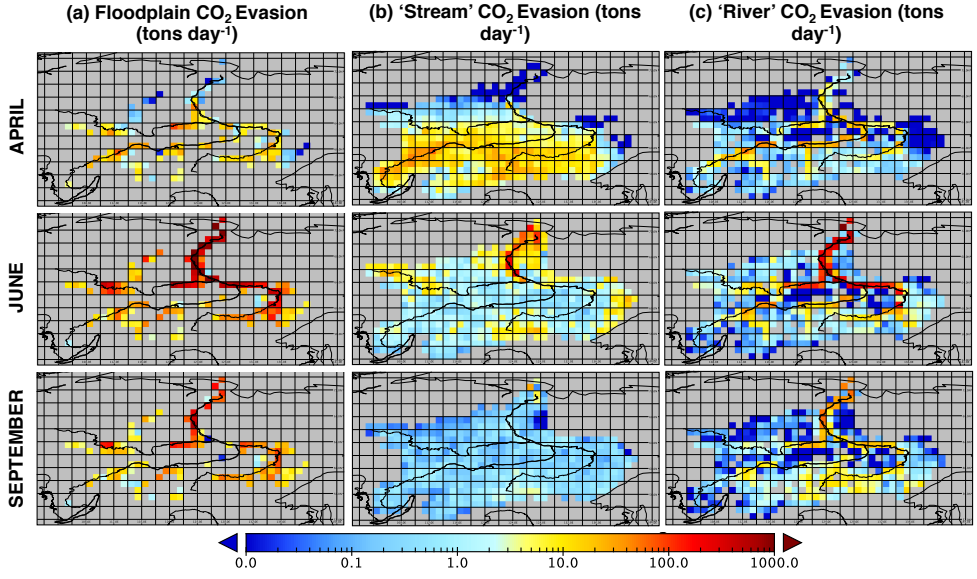

Figure 8: Maps of CO_2 evasion from the surface of the three surface hydrological pools, (a) the floodplains, (b) streams and (c) rivers in April, June and September. All maps use the same (log) scale in units of (tons $pixel^{-1}$ d^{-1}).

Geosci. Model Dev. Discuss., https://doi.org/10.5194/gmd-2018-322
Manuscript under review for journal Geosci. Model Dev.
Discussion started: 25 March 2019

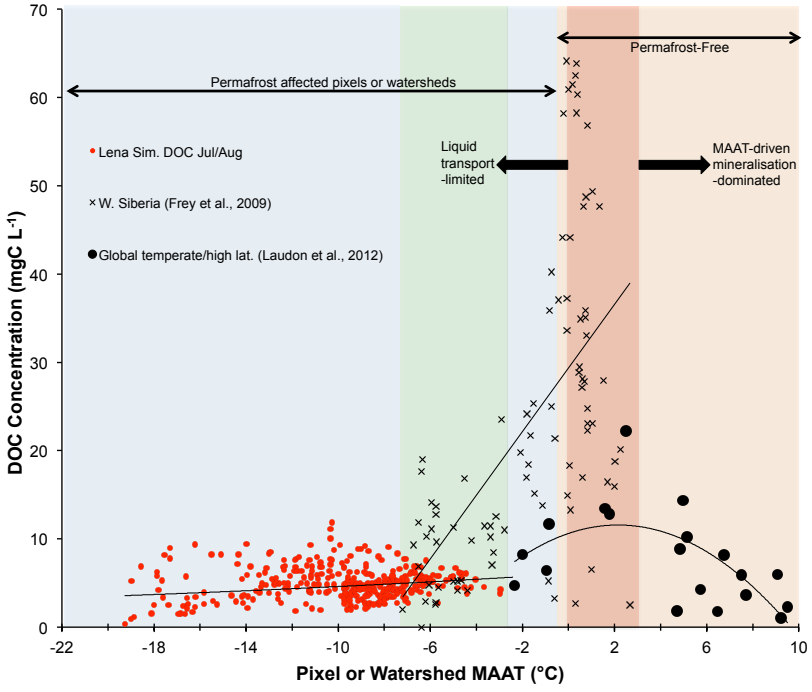

Figure 9: Mean summertime DOC concentrations (mgC L^{-1}) plotted against mean annual air temperature (MAAT, °Celsius) for simulated pixels over the Lena river basin (red circles), and observations for largely peat-influenced areas in western Siberia as reported in Frey et al., 2009 (black crosses), and observations from a global non-peat temperate and high latitude meta-analysis (black circles) reported in Laudon et al. (2012). The blue region represents permafrost-affected areas, while the orange region represents permafrost-free areas. The green region bounds the area of overlap in MAAT between the observed and simulated datasets. The dark red shaded area corresponds to the MAAT 'zone of optimality' for DOC production and transport proposed by Laudon et al. (2012). Regression curves of DOC against MAAT for each of the separate datasets are shown for each individual dataset.

Geosci. Model Dev. Discuss., https://doi.org/10.5194/gmd-2018-322
Manuscript under review for journal Geosci. Model Dev.
Discussion started: 25 March 2019

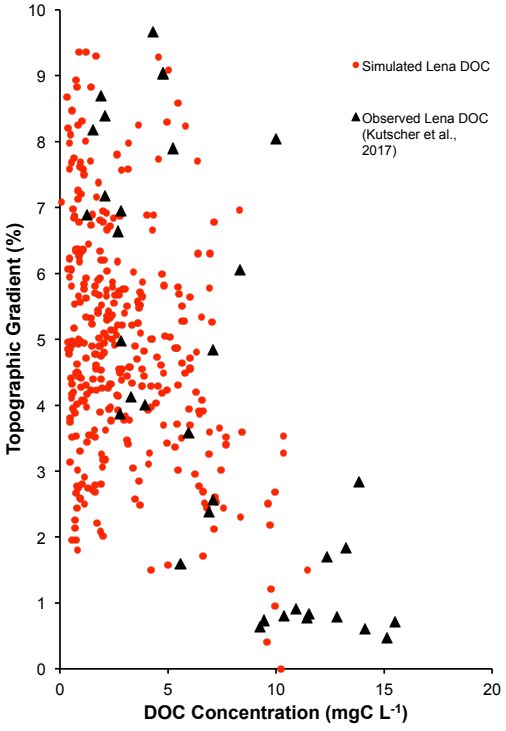

Figure 10: Variation of DOC concentrations versus topographic slope in Kutscher et al., 2017 (black triangles) and (red dots) as simulated and averaged for the summer months (JJA) over 1998-2007; observed values were measured during June and July 2012-2013.

(a)

Geosci. Model Dev. Discuss., https://doi.org/10.5194/gmd-2018-322
Manuscript under review for journal Geosci. Model Dev.
Discussion started: 25 March 2019

Geoscientific Model Development Discussions
Open Access
EGU

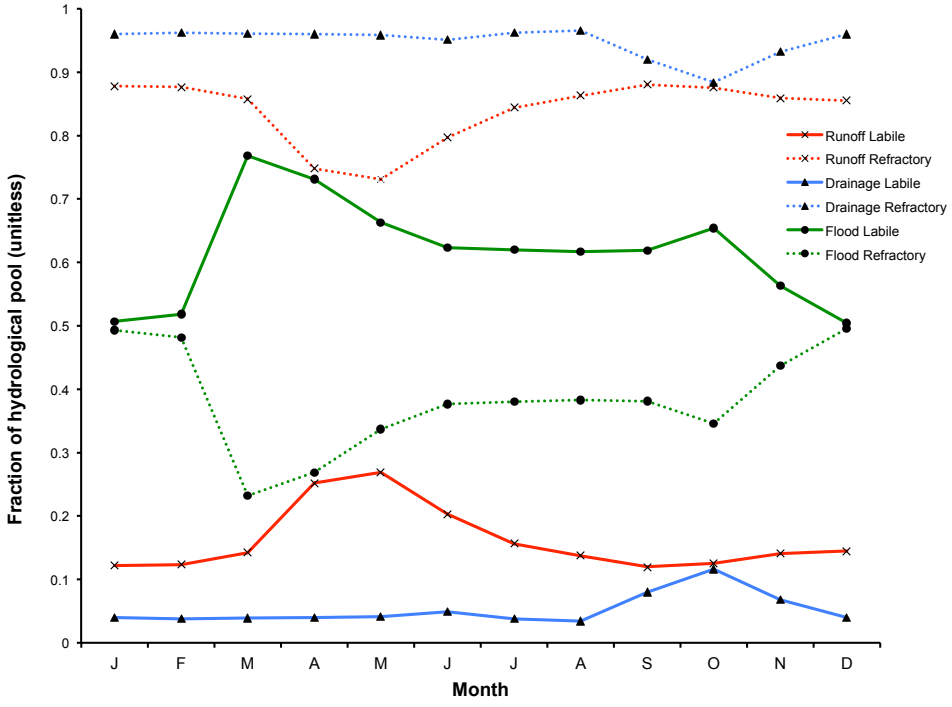

1411
1412 **(b)**
1413

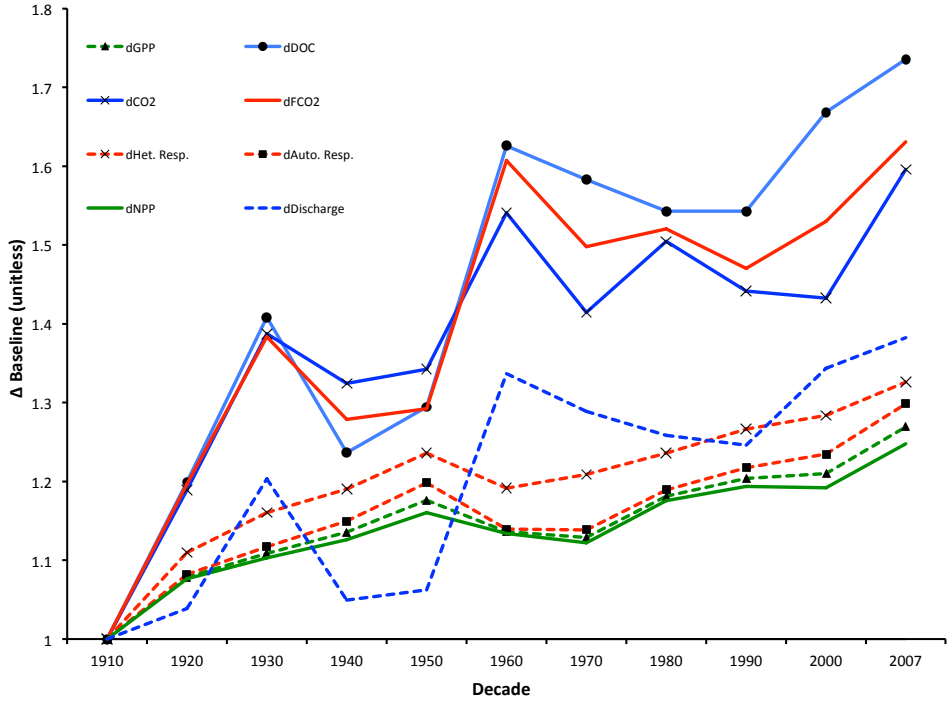

1414

Geosci. Model Dev. Discuss., https://doi.org/10.5194/gmd-2018-322
Manuscript under review for journal Geosci. Model Dev.
Discussion started: 25 March 2019

1415 **(c)**

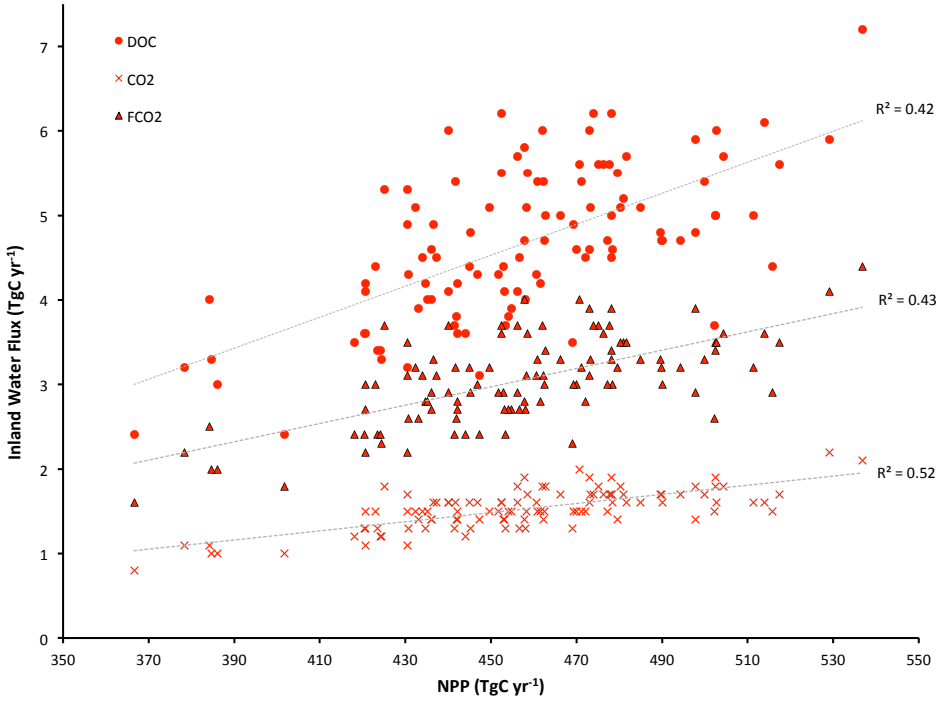

1416
1417 **Figure 11:** (a) The mean monthly fraction of each hydrological pool's (runoff, drainage,
1418 floodplains) carbon reactivity constituents (labile and refractory) averaged across the
1419 simulation area over 1998-2008. **(b)** Time series showing the decadal-mean fractional
1420 change in carbon fluxes normalised to a 1901-1910 average baseline (=1 on the y-axis)
1421 for NPP, GPP, autotrophic and heterotrophic respiration, DOC inputs to the water
1422 column, CO_2 inputs to the water column, CO_2 evasion from the water surface (FCO2), and
1423 discharge. **(c)** Summed yearly lateral flux versus NPP values for DOC discharge, CO_2
1424 discharge and CO_2 evasion (FCO2) over the entire simulation period, with linear
1425 regression lines shown.
1426

Geosci. Model Dev. Discuss., https://doi.org/10.5194/gmd-2018-322
Manuscript under review for journal Geosci. Model Dev.
Discussion started: 25 March 2019

1427 **(a)**

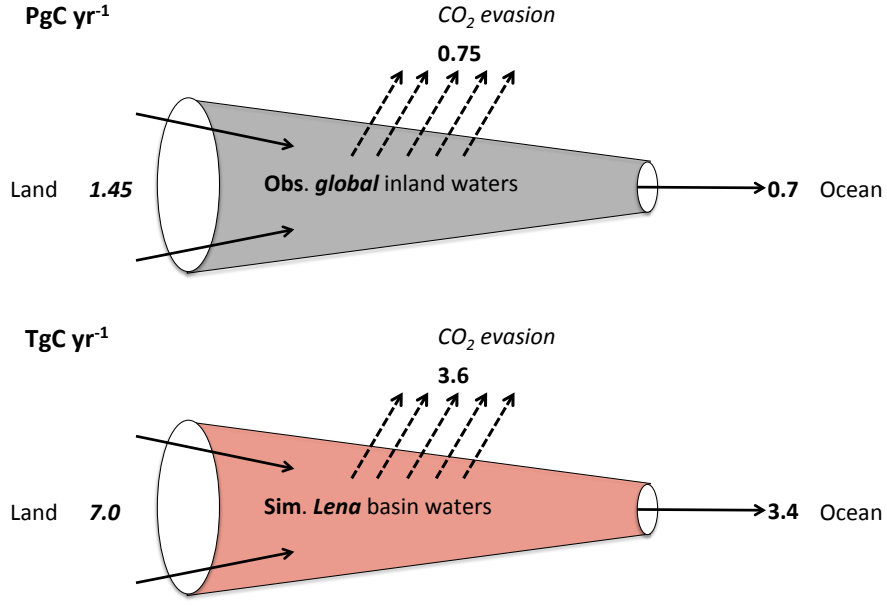

1428
1429 **(b)**

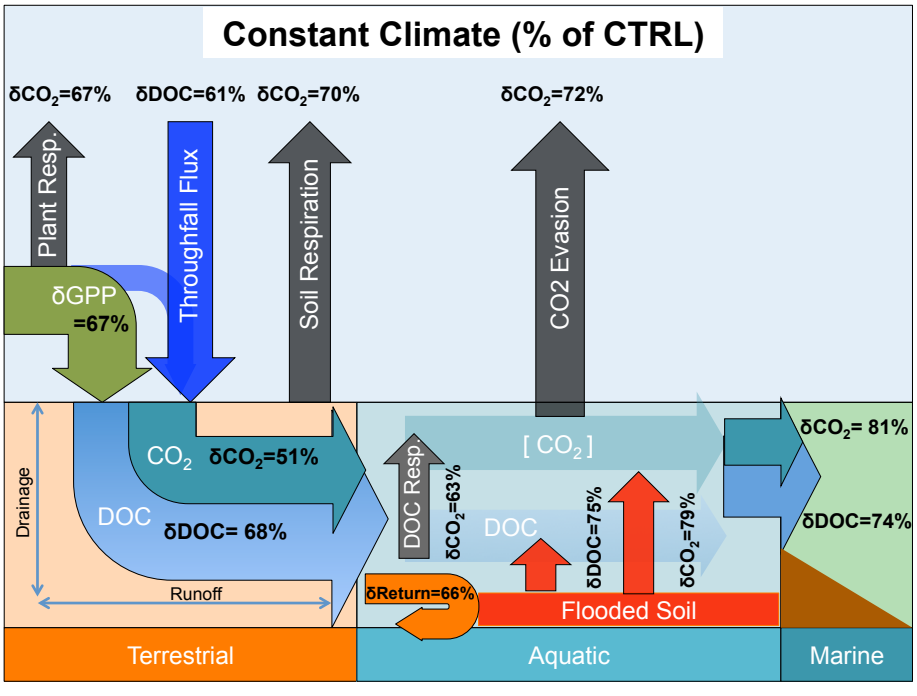

1430
1431 **(c)**

Geosci. Model Dev. Discuss., https://doi.org/10.5194/gmd-2018-322
Manuscript under review for journal Geosci. Model Dev.
Discussion started: 25 March 2019

Geoscientific Model Development Discussions

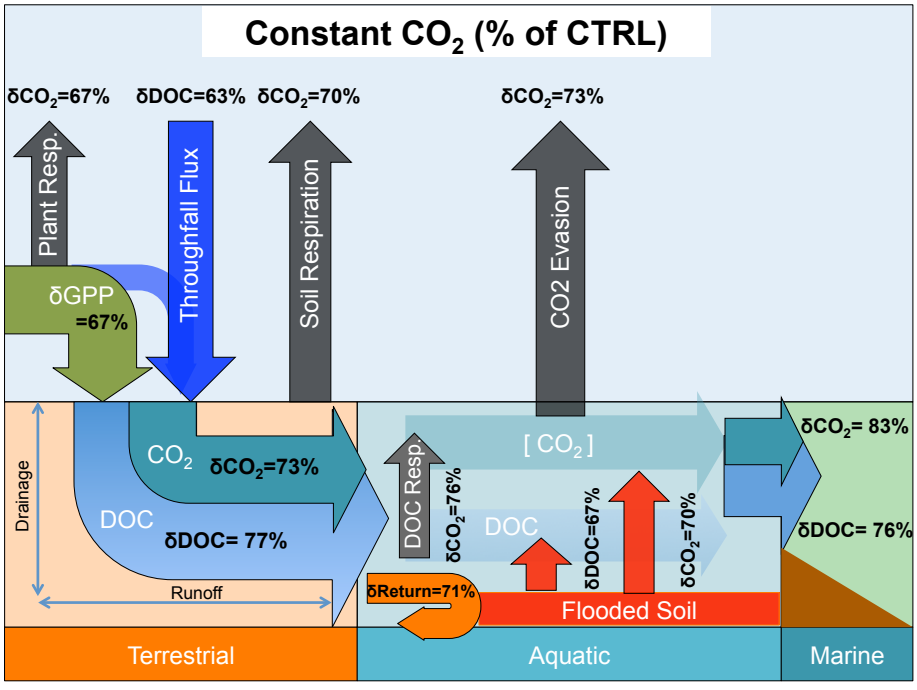

Figure 12: **(a)** Simplified 'leaky pipe' diagram representing the transport and processing of DOC within the land-ocean hydrologic continuum. The scheme template is taken from Cole et al. (2007), where we reproduce their global estimate of DOC and non-groundwater discharge portion of this flow in the top panel (PgC yr^{-1}), and the equivalent flows from our Lena basin simulations in TgC yr^{-1} in the bottom panel. Thus easy comparison would look at the relative fluxes within each system and compare them to the other. **(b-c)**: Schematic diagrams detailing the major yearly carbon flux outputs from simulations averaged over the period 1998-2007 as they are transformed and transported across the land-aquatic continuum. Figures **(b)** and **(c)** give the same fluxes as a percentage difference from the Control (CTRL-Simulation), for the constant climate and CO_2 simulations, respectively.

Geosci. Model Dev. Discuss., https://doi.org/10.5194/gmd-2018-322
Manuscript under review for journal Geosci. Model Dev.
Discussion started: 25 March 2019

Geoscientific Model Development Discussions

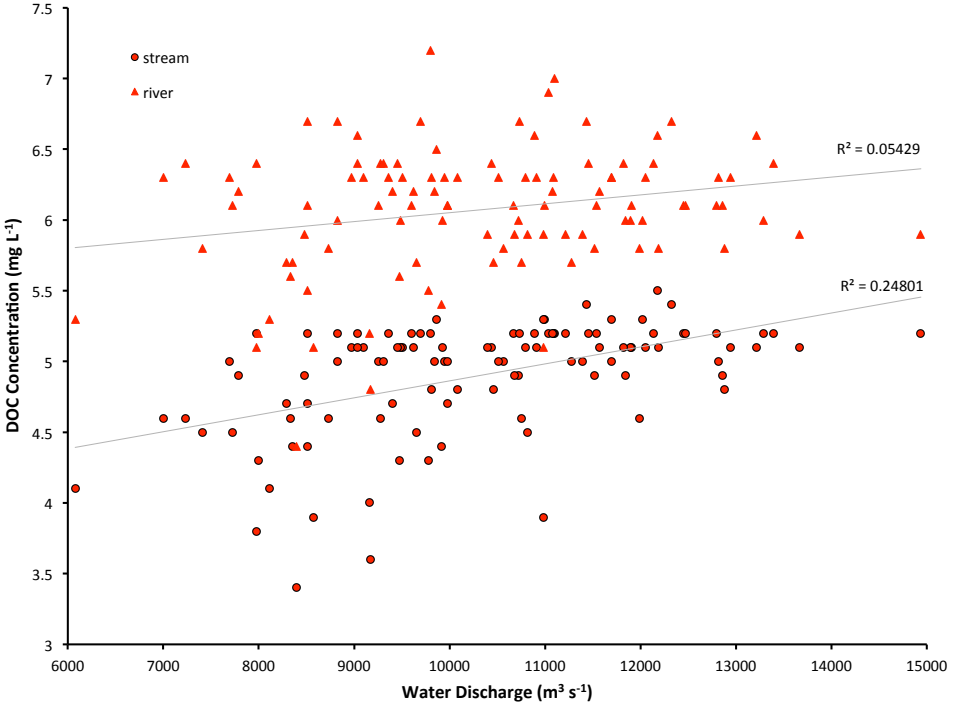

Figure 13: Simulated basin-mean annual DOC concentrations (mg L^{-1}) for the stream and river water pools regressed against mean annual simulated discharge rates (m^3 s^{-1}) at Kusur over 1901-2007. Linear regression plots with corresponding R^2 values are shown.